Monte Carlo Simulations of Neutrons Interaction with LiF and Boron Converters

Optimisation of multilayered GEM detectors and response characterisation

Lina Quintieri

CERN, Geneva, 16-17 March 2015

Outlook

- Context of the work and MC general remarks

- FLUKA, Geant4, a brief description on hadron physics and secondary ions transport

- B-10 converter layer: application on GEM SideOn neutron detector design and optimisation by MC codes.

- Comparison of MC efficiency predictions for "5 plates GEM SideOn" prototype detector configuration vs. experimental results

- LiF converted layer: preliminary results on single plate case (conversion efficiency vs. thickness, secondary charged particle spectrum vs. thickness, etc) and comparison with B-10 equivalent thickness resulst

- Conclusions & on-going activities

He-3 Crisis and Development of New Efficient Neutron Detectors

❖ ^{3}He is obtained from Tritium production for use in nuclear weapons by Tritium ß-decay into ^{3}He with a half life of 12.3 years.

❖ Only the US and Russia are providing significant amounts of ^{3}He. With the end of the Cold War ^{3}He production from Tritium decay has been reduced significantly and since September 2001 the demand of ^{3}He has increased drastically due to security program launched in US and other countries.

❖ **Severe depletion** of the existing ^{3}He stockpile and shortage

❖ Cost increase by a **factor of 25**: from 80 €/l up to 2000 €/l

❖ ^{3}He demand for neutron scattering in **2009 – 2015 is estimated to 125 kl** and the projected demand for US security applications is 100 kl. For a ≈**20 kl/year available** (US + Russia).

In this frame it is easy to understand the strong importance of MC simulations as a valuable and "costless" tool to address the research toward new neutron valuable detector in alternative to the ^{3}He.

MC Methods: General Remarks

❖ Deterministic methods provide more exact solutions of approximate models, whereas **Monte Carlo methods provide approximate solutions of more exact models (stochastic events)**

❖ MC method is **eminently suited to study stochastic processes**, particularly radiation transport, such as motion of photons and neutrons and charged particles through matter.

❖ Monte Carlo simulations play an important role in the optimisation particle detector design..The method uses **probabilities distribution functions** and **random sampling** instead to give an accurate picture of what can happen. Statistically the random samplings will most often demonstrate the most likely possibilities

❖ **The accuracy and reliability of a Monte Carlo predictions depends on the models or evaluated data libraries** on which the probability distribution functions are based

❖ Often variance reduction techniques are required to improve the result accuracy and accelerate the statistical convergence(increasing statistics using weight for secondaries, in order to not affect the physics)

❖ The Monte Carlo **design of a neutron detector relies** on the MC **ability to track the charged secondary particles produced**: (n,α), (n,p), (n,f) etc

❖ Experimental verification would not only be difficult to accomplish but expensive as well. Monte Carlo allows us to simulate an actual physical experiment and look at what most likely will happen. This information helps us to optimize the detector without actually building it.

❖ **Separate unseparable effect: create unrealistic cases to help better understanding problems**

MC Errors and Limitations

❖ The Monte Carlo method involves calculating the average or probable behaviour of a system by observing the outcomes of a large number of trials (histories), after simulating the physical events responsible for the behaviour (on the base of physical model or evaluated data libraries).

❖ **MC simulations always have some errors which arise from the nature itself of the calculations**.

❖ **Statistical precision of results** depends on the number of "histories"(in analogue mode: **1/√N**)

❖ Moreover there are errors due to

❖ discrepancies, between the reality and the implementation, in material composition and geometry

❖ errors in nuclear data libraries and theoretical models

❖ ….other

MC General Transport Assumptions

❖ Static, homogeneous, isotropic, and amorphous media (and geometry)

❖ Markovian process: the fate of a particle depends only on its actual properties, not on previous events or history

❖ Particles do not interact with each other

❖ Particles interact with individual atoms/nuclei/molecules (not true at low energies)

❖ Material properties are not affected by particle reactions (but dpa can be estimated)
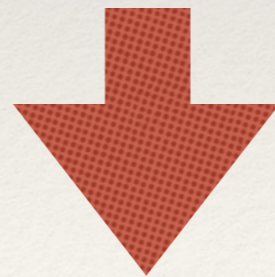
The superposition principle can be used

Fluka & Geant4

They are general-purpose Monte Carlo code that can reproduce geometric 3D configurations of materials and simulate particle transport through them

General	GEANT	FLUKA
UPDATE VERSION	Geant4.10	Fluka 2011.2c
LANGUAGE	C++	Fortran 77
RELEASE FORMAT	Source & binary	Binary
INPUT FORMAT	N/A	~85 cards
PARALLEL EXECUTION	YES	YES

Fluka & Geant4: Physics Capabilities

(ref: G. McKinney et al. proc Science)

PHYSICS		GEANT	FLUKA
Particles		68	68
Charged particles		CSDA	CSDA
Energy loss		Bethe-Bloch	Bethe-Bloch
Scatter		Lewis	Moliere improved
Straggling		Urban	Custom
XTR/Cheren.		Yes	No/yes
Neutron	Low	Cont. (ENDF)	Multigroup(260) **
	High	Models	Models
Proton	Low & High	Models	Models
Leptons	Electron	Models/EEDL, EADL	Custom
	Muon	Models	Models
	Neutrino	Production	Models
	Other	Decay	Decay
Photons Optical		YES	YES
x-ray/g		Models or EPDL97, EADL	Custom+EPDL97
Photonuclear		CHIPS	PEANUT
Fields (E/B)		YES	YES

(**) In Fluka, for a few isotopes only, neutron transport can be done also using continuous (pointwise) cross sections. For H, Li6 and B-10, it is applied as a user option (above 10 eV in H, for all reactions in Li6, and only for the reaction B-10(n,a)Li7 in B-10). For the reaction 14N(n,p)14C, pointwise neutron transport is always applied.

A Quick Look Inside the Codes: Highlight on Differences

FLUKA Hadron Physics and Secondary Ions Transport

❖ In FLUKA, **recoil protons and protons from N(n,p)** reaction **are produced and transported explicitly**, taking into account the detailed kinematics of elastic scattering, continuous energy loss with energy straggling, delta ray production, multiple and single   scattering.

❖ **The same applies to light fragments (α,triton) from neutron capture in L6 and B-10, if point-wise transport has been requested by the user.** All other charged secondaries, **including fission fragments,** are not transported but their energy is deposited **at the point of interaction (kerma approximation).**

❖ Correlation issue when based on evaluated data files. Non-correlation between energy and angle for secondary particles produced by neutrons in inelastic processes (with gamma emission). **It would be preferable to use theoretical models do describe the physical process, when possible.**

Particle transport limits in FLuka

Particle	Secondary particles	Primary particles
charged hadrons	1 keV-20 TeV	100 keV-20 TeV
neutrons	thermal-20 TeV	thermal-20 TeV
antineutrons	1 keV-20 TeV	10 MeV-20 TeV
muons	1 keV-1000 TeV	100 keV-1000 TeV
electrons	1 keV-1000 TeV	70 keV-1000 TeV (low-Z materials) 150 keV-1000 TeV (hi-Z materials)
photons	100 eV-10000 TeV	1 keV-10000 TeV
heavy ions	<10000 TeV/n	1 keV-10000 TeV

Geant4 Hadron Physics and Secondary Ion Transport

❖ Geant4 applies a string model for the modeling of interactions of high energy hadrons, i.e. for protons, neutrons, pions and kaons above ~(5-25) GeV depending on the exact physics list.

❖ Interactions at lower energies are handled by one of the intranuclear cascade models or the precompound model. Nuclear capture of neutrons at rest is handled using either the Chiral Invariant Phase Space (CHIPS) model or the Bertini intranuclear cascade

❖ **For inelastic scattering, the currently supported final states are (nA→) nγs (discrete and continuum), np, nd, nt, n3He, nα, nd2α, nt2α, n2p, n2α, npα, n3α, 2n, 2np, 2nd, 2nα, 2n2α, nX, 3n, 3np, 3nα, 4n, p, pd, pα, 2p d, dα, d2α, dt, t, t2α, 3He, α, 2α, and 3α.**

Particle transport limits in Geant4

❖ **In Geant4 there are no tracking cuts: particles are tracked down to a zero range/kinetic energy**

❖ **Only production cuts** exist: i.e. cuts allowing a particle to be born or not

❖ The production of a secondary particles is relevant if it can generate visible effects in the detector , otherwise "local energy deposit"

❖ A range cut allows to easily define such visibility

  ❖ "we want to produce particles able to travel at least 1 mm (if particle can travel less than 1mm they are no more transported but dye depositing locally their energy)". The criterion can be applied uniformly across the detector

❖ Each particle (G4ParticleWithCut) converts the range cut into an energy cut, for each material: processes then compute the cross-sections based on the energy cut

Particle transport limits in Geant4

Particle	Particle upper limit transportation
charged hadrons	<100 TeV
neutrons	< 20 TeV
muons	< 1 PeV
electrons	< 100TeV 250 eV-1GeV (Livermore library)
photons	< 100TeV
heavy ions	< 100TeV

Simulating α and Li ion production and transport: summary of user activated options

Fluka

In order to explicitly produce an α and Li7 ion pair from the neutron interaction on B-10, it is needed to:

❖ define a monoisotope material named BORON-10 and associated to it the B-10 low energy cross section (<20 MeV)

❖ Activate the ion transport (i.e. α and Li7) with IONTRANS card and set an **appropriate ion transport threshold** with **PART-THR** applied to 4-HELIUM (Li7 will get the same energy per nucleon threshold)

❖ Choose the **option Point wise-XS in LOW-NEUT** transport card: this is available and possible only for few isotopes: B-10 and Li6

❖ Boundary crossing current estimator (USRBDX)To score α and Li7's leaving the converter use a.

Geant4

QGSP_BIC_HP() referenced physics list has been chosen

In this physics list, the Geant4 Binary cascade for primary protons and neutrons with energies below ~10GeV: Binary cascade better describes production of secondary particles produced in interactions of protons and neutrons with nuclei.

Applicative cases:
design and optimisation of B-10 and LiF converter material based detectors

B-10 Cathode: MC Optimisation of "Gem SideOn" Detector Design
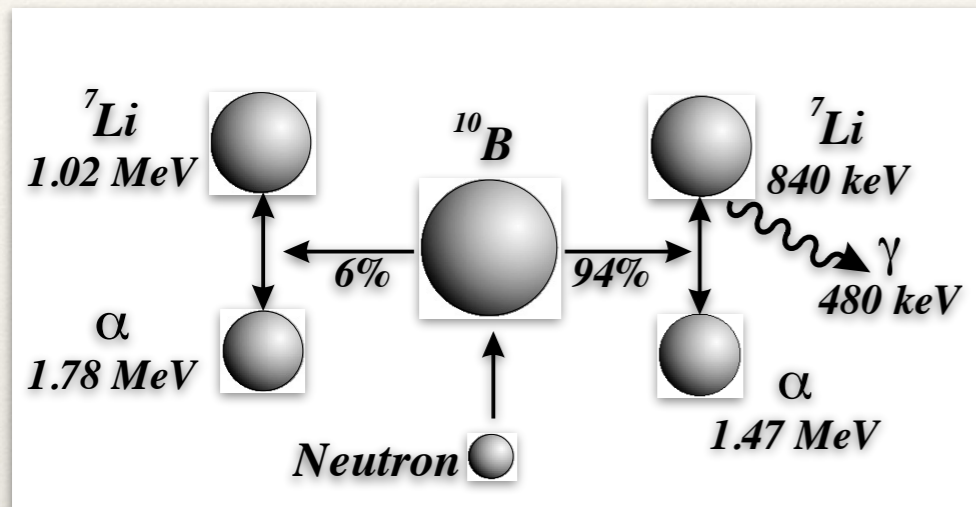
The reaction products are released in opposite direction when thermal neutrons are absorbed by B-10.

After the absorption 94% of the reactions leave le Li7 in its first excited state, which rapidly de-excite to the ground (10^-13s) by releasing a 480 keV gamma).
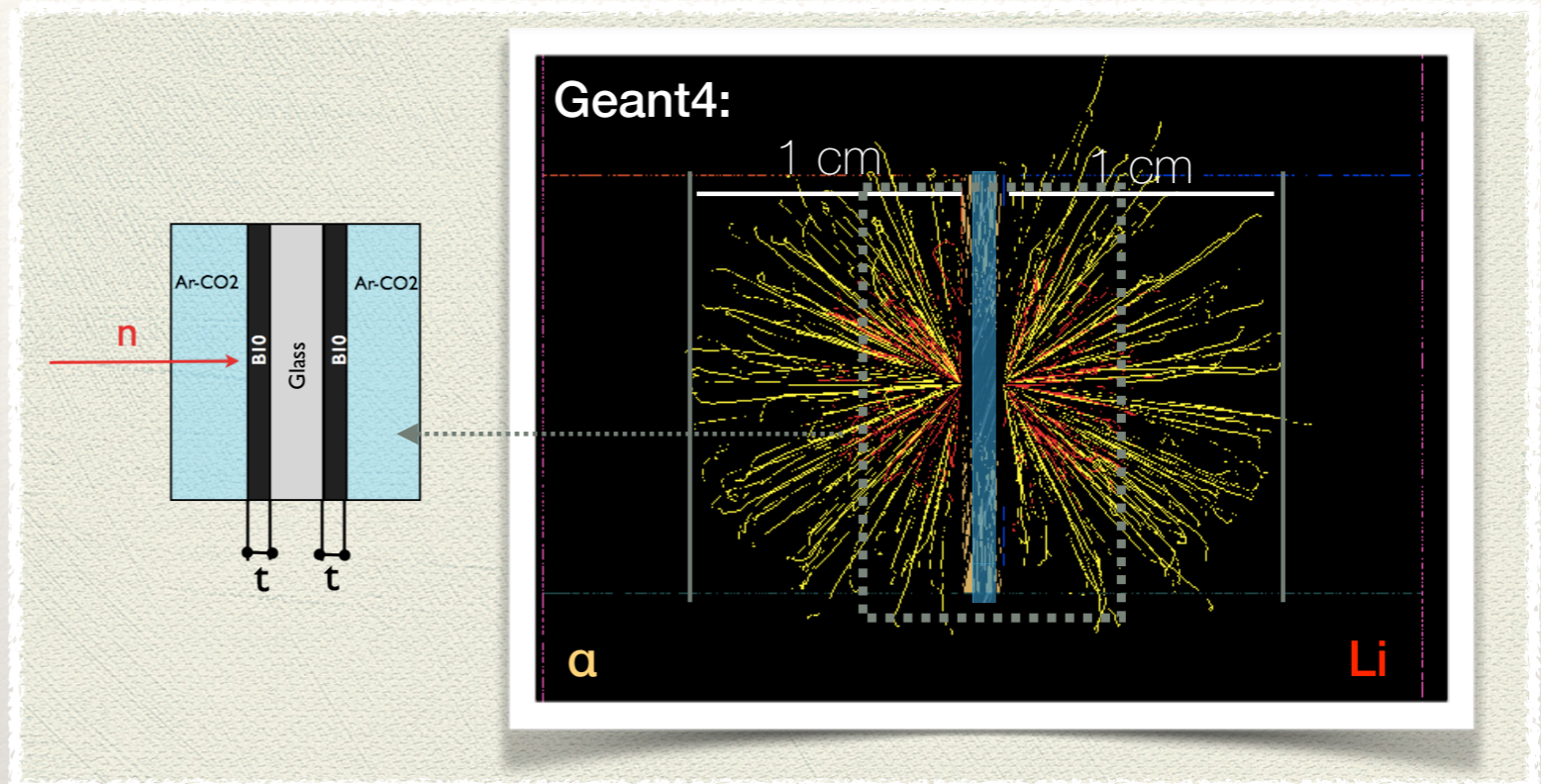
Results of simulations,shown in figure, refer to Al2O3 plate coated (on both sides) with nat-B uniform layers in ArCO2 hit by thermal neutron.

A primary (25 meV) neutron beam impinges perpendicular to the wider sheet surface, (zero divergence)

The simulations intended to help in seeking the optimal geometrical set-up and material thickness (converter layer, gas gap, sheet substrate) to improve the final detector design in terms of achieving the best detector efficiency possible.

B-10 Cathode: MC Optimisation of "Gem SideOn"
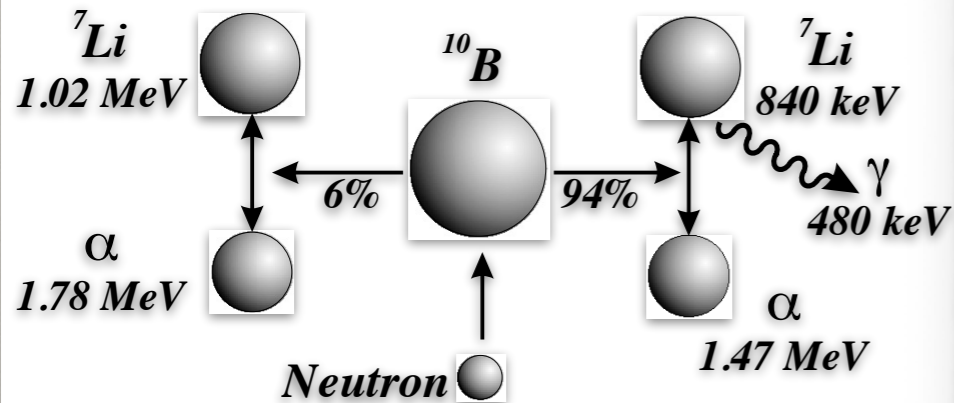
The reaction products are released in opposite direction when thermal neutrons are absorbed by B-10.

After the absorption 94% of the reactions leave le Li7 in its first excited state, which rapidly de-excite to the ground (10^-13s) by releasing a 480 keV gamma).

Refer to the A. Pietropaolo talk for more details on this work

A new ^{3}He-free thermal neutrons detector concept based on the GEM technology

A. Pietropaolo [a,*], F. Murtas [b], G. Claps [b], L. Quintieri [b,1], D. Raspino [c], G. Celentano [d], A. Vannozzi [d], O. Frasciello [b]

a Consiglio Nazionale delle Ricerche, Istituto di Fisica del Plasma "P. Caldirola", Milano, Italy
b Istituto Nazionale di Fisica Nucleare, Laboratori Nazionali di Frascati, Frascati, Italy
c Science and technology Facility Council, ISISI Facility, Chilton, Didicot, United Kingdom
d ENEA Centro Ricerche Frascati, Frascati, Italy

ARTICLE INFO

ABSTRACT

A thermal neutron detector based on the Gas Electron Multiplier technology is presented. It is configured to let a neutron beam interact with a series of borated glass layers placed in sequence along the neutron path inside the device. The detector has been tested on beam both at the ISIS (UK) spallation neutron source and at the TRIGA reactor of ENEA, at the Casaccia Research Center, near Rome in Italy. For a complete characterization and description of the physical mechanism underlying the detector operation, several Monte Carlo simulations were performed using both Fluka and Geant4 code. These simulations are intended to help in seeking the optimal geometrical set-up and material thickness (converter layer, gas gap, sheet substrate) to improve the final detector design in terms of achieving the best detector efficiency possible.

thermal neutron.

A primary (25 meV) neutron beam impinges perpendicular to the wider sheet surface, (zero divergence)

The simulations intended to help in seeking the optimal geometrical set-up and material thickness (converter layer, gas gap, sheet substrate) to improve the final detector design in terms of achieving the best detector efficiency possible.

# From Single Sheet Validation to Efficiency Prediction for the Complete Detector

We took a **simple geometry** to push the physics: a single sheet with thin two-side converter layer.

Since Boron is resistive, the accumulate charge in the boron layer is not an issue, so that the conversion efficiency can be defined as: the charged particle that enter into the gas per unit absorbed neutron

In this case the **theoretic conversion efficiency** and secondary particle distribution could be easily estimated (all the charged particles enter into the gas)

As the B-10 thickness increases, the **number of charged particles produced differs from the number of charged particles that reach the gas** region and this effect becomes appreciable for B-10 thickness much lower than the α and Li7 range values: the range of 1.47 MeV αs and 0.84 MeV Li7 ions in B-10 is respectively about 3.6 μm and 2 μm).

Starting point: validation of the single sheet (300nm B-10)
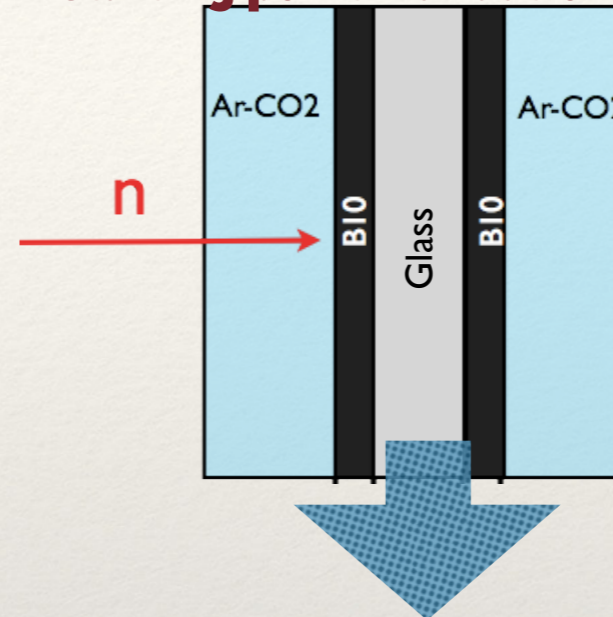
The neutron beam impinges laterally onto the detector rather than onto the cathode, as typically happens in almost all GEM-based detectors applications.

goal: to optimize the multiple sheet final design
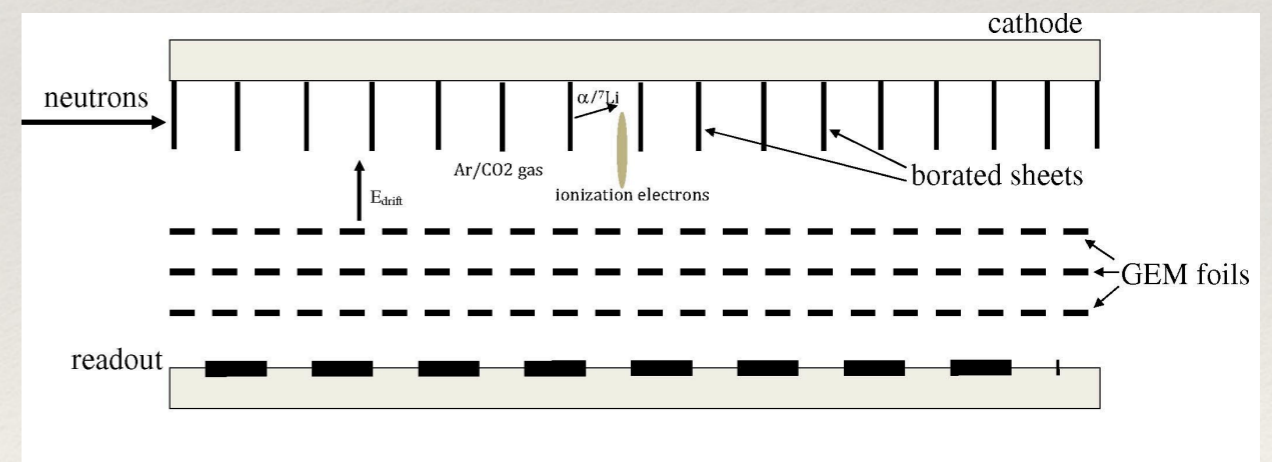
The charged particles ionize the Ar/CO2 gas mixture in the drift region. The secondary electrons, moved by the electric field in this region, reach the three GEM foils where they are further multiplied

Geometry and interacting neutron beam
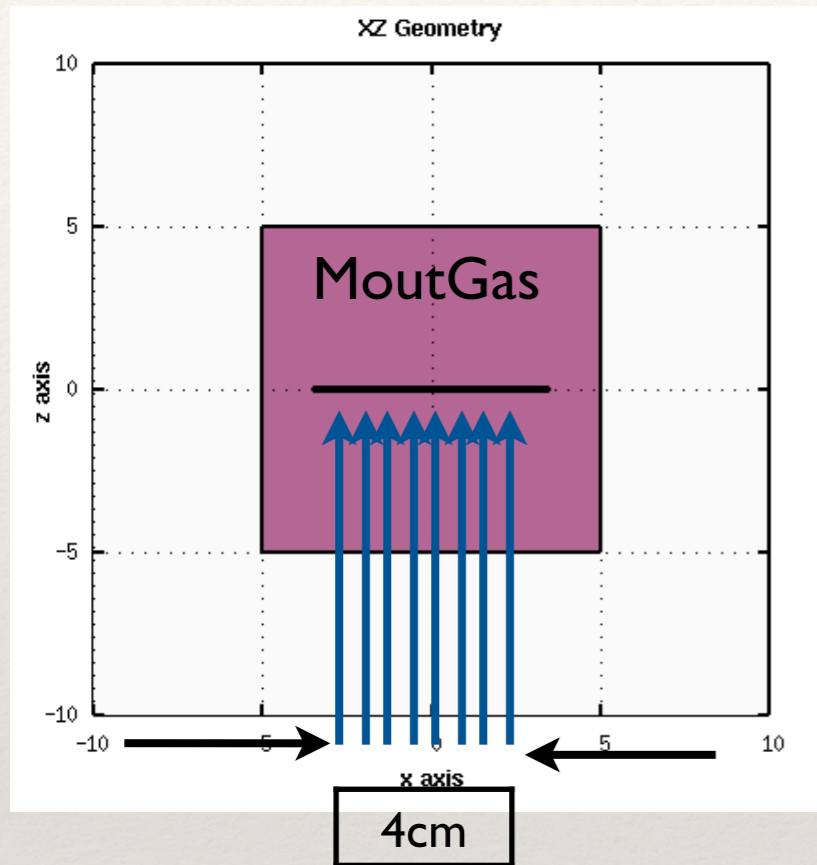
| Region	Dx	Dy	Dz
galss	7cm	1cm	0.1cm
B-10 Layer	7.cm	1cm	3E-5cm
active gas	10cm	1cm	10cm

Neutron beam: primary and scattered particles
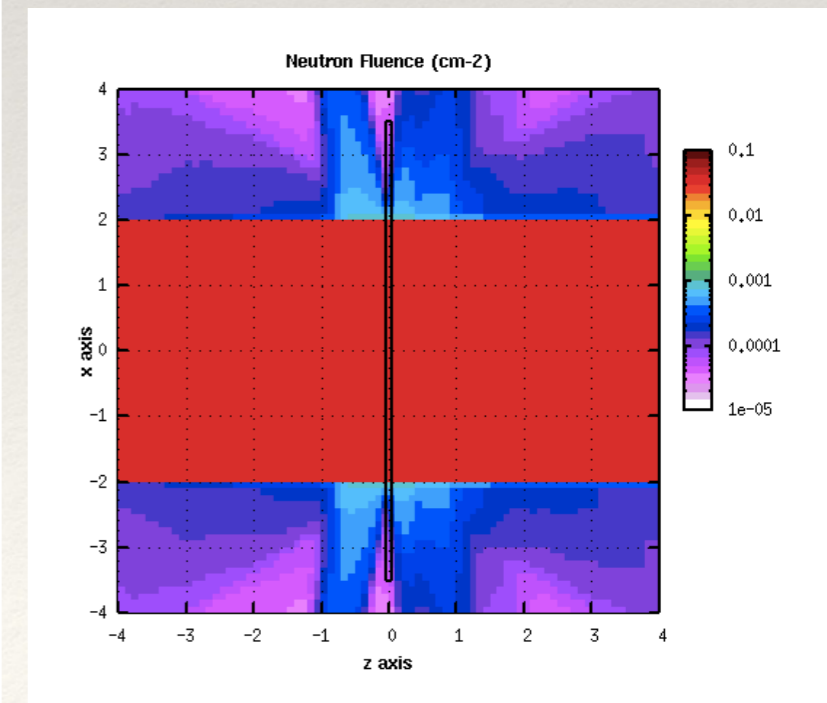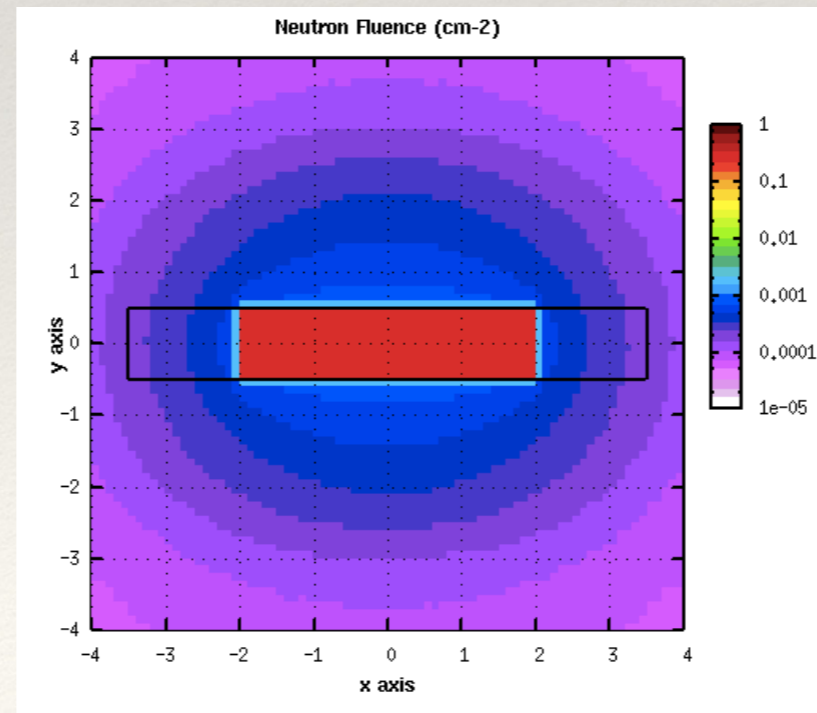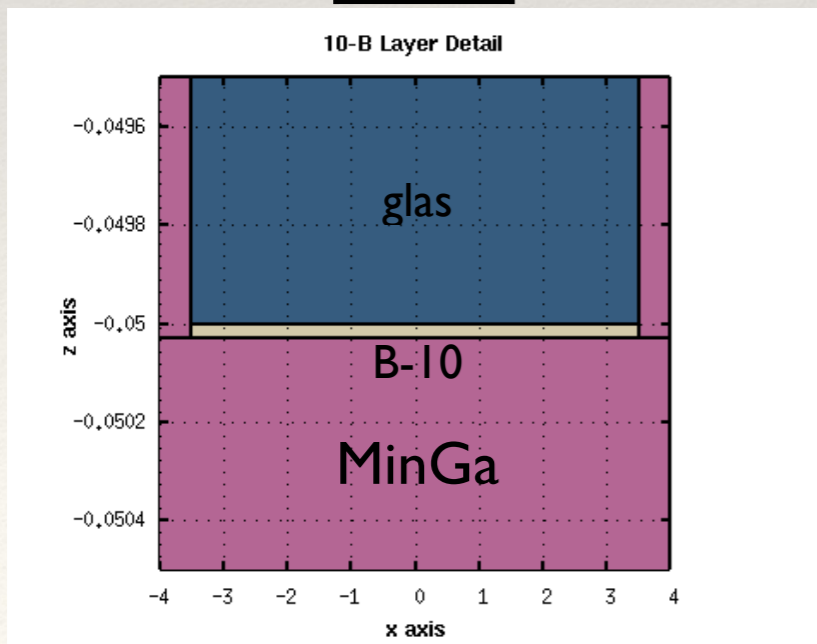
Spatial Energy Deposition and Particle Fluences: Detailed Results for a 300 nm B-Coated Single Sheet

Case of a rectangular uniform thermal neutron beam

Predicted energy deposition by the charged particles in the gas, for different converter thickness values (from 300 up to 1200 nm).
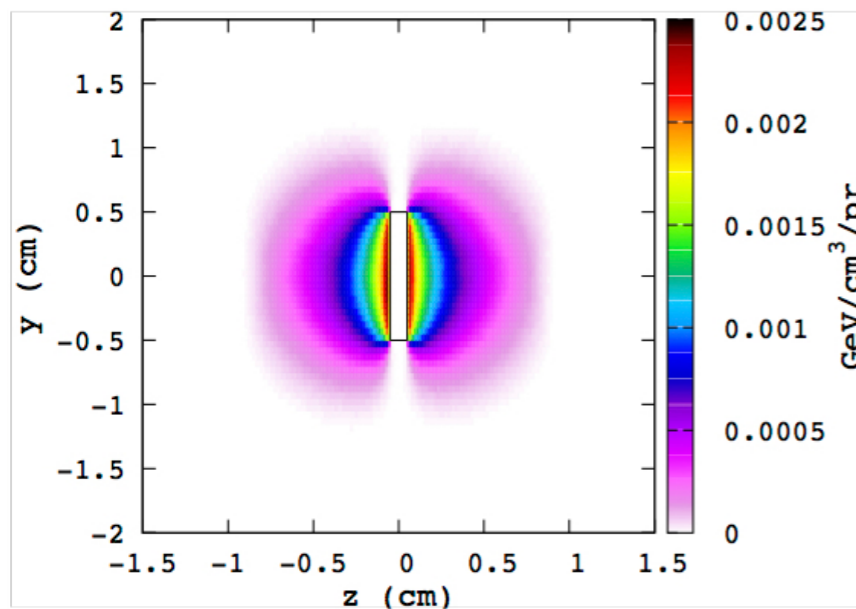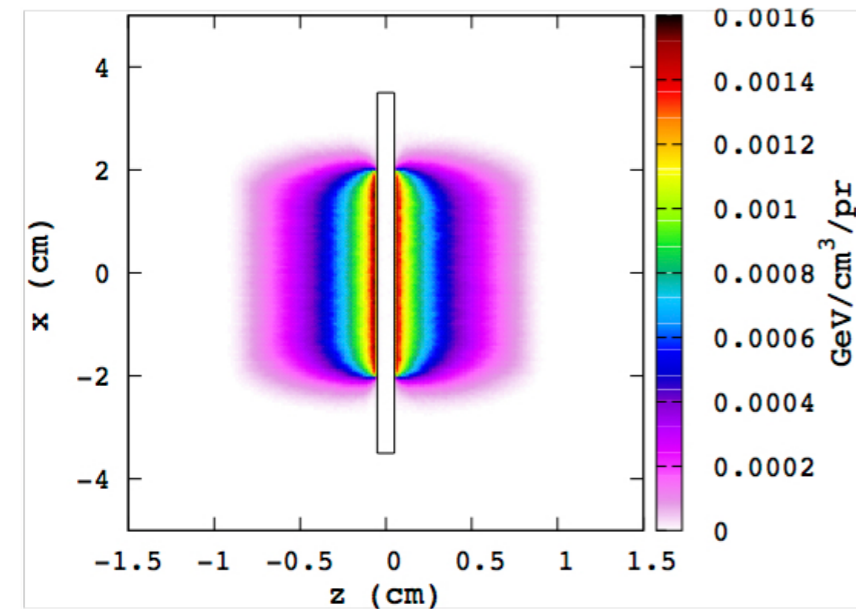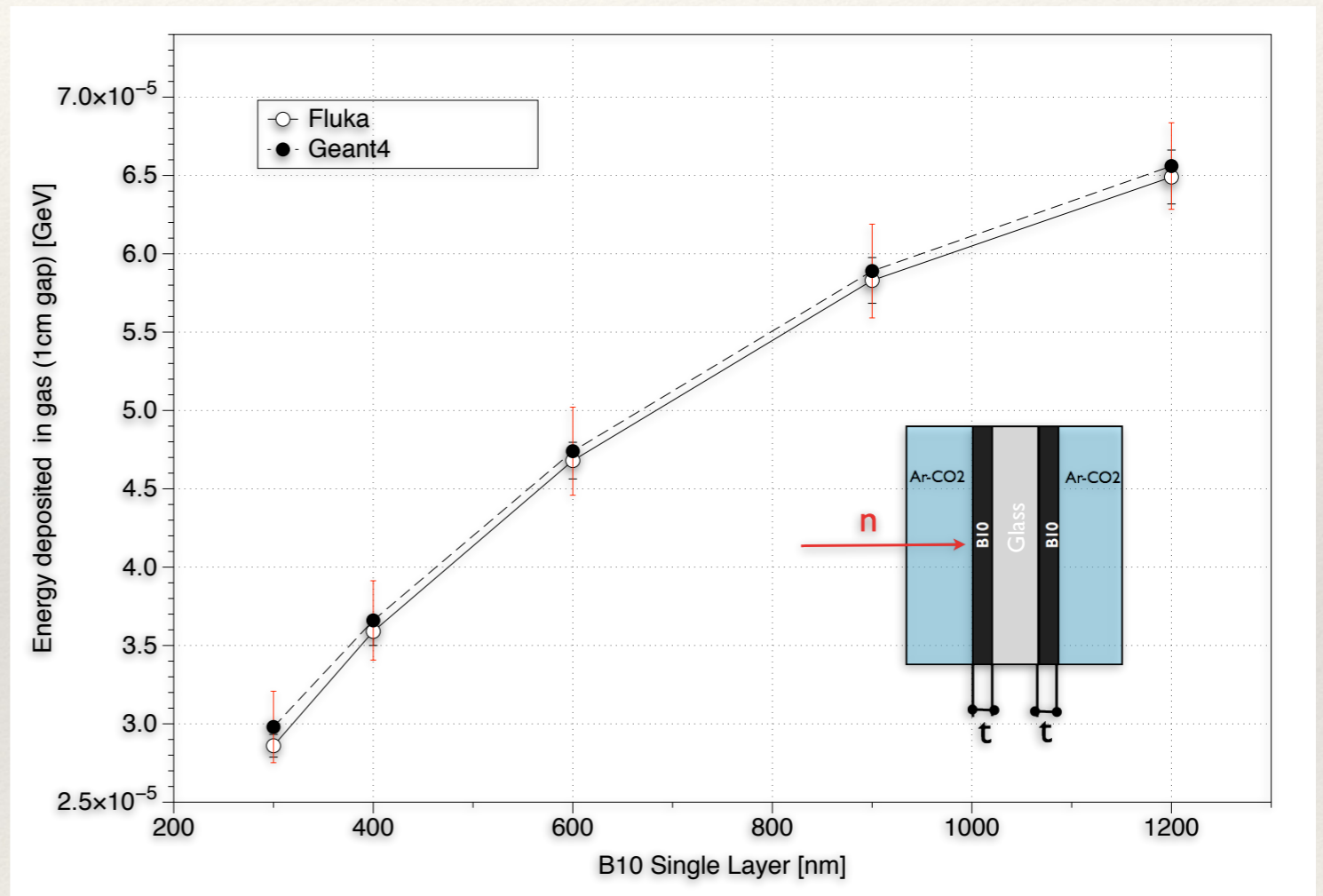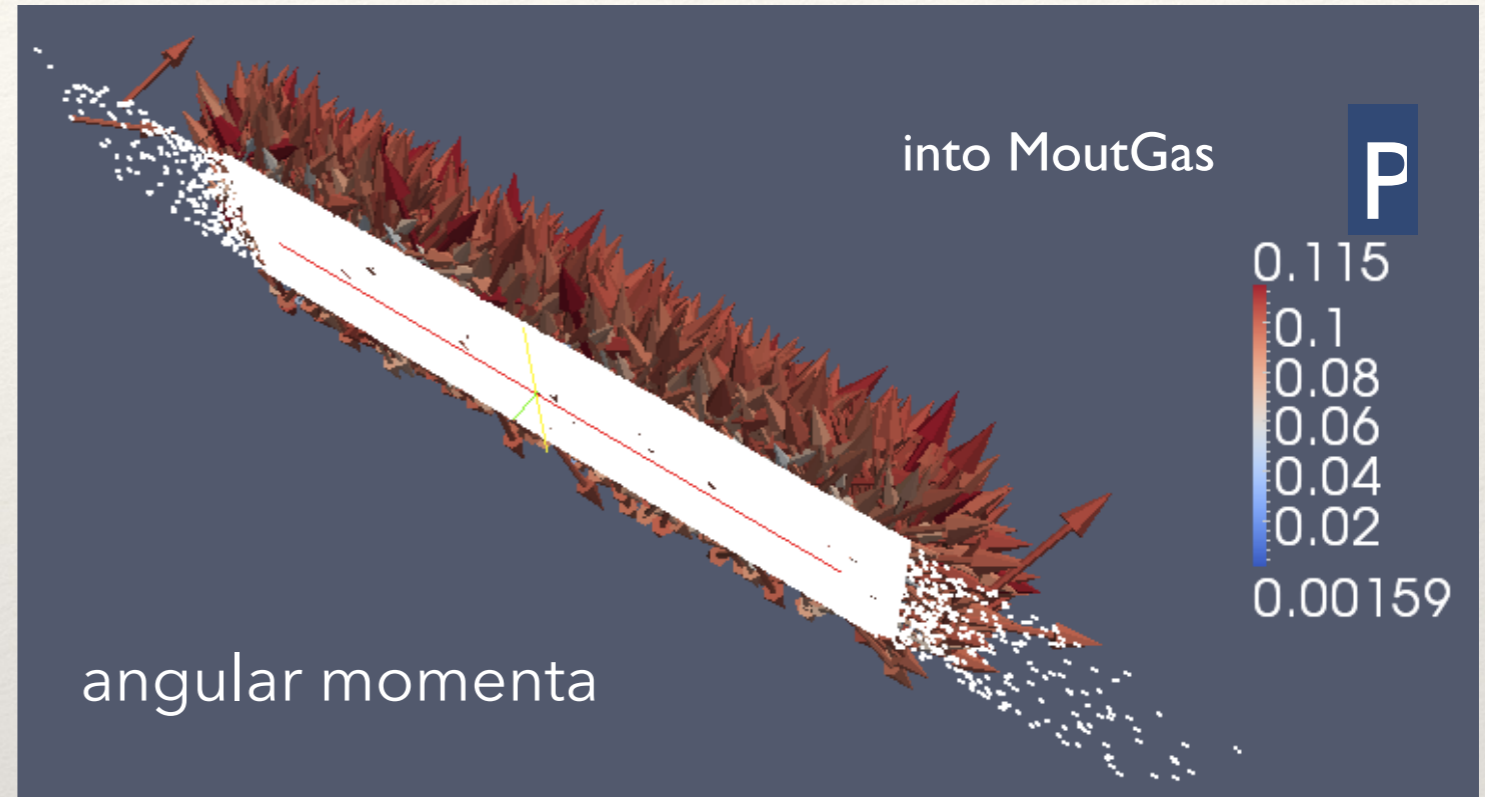

Good agreement between the Geant4 and Fluka predictions.

To highlight: increasing the B-10 thickness **by a factor of 4** (from 300 nm to 1200 nm) the energy deposited in the gas increase only by a **factor of 2**.
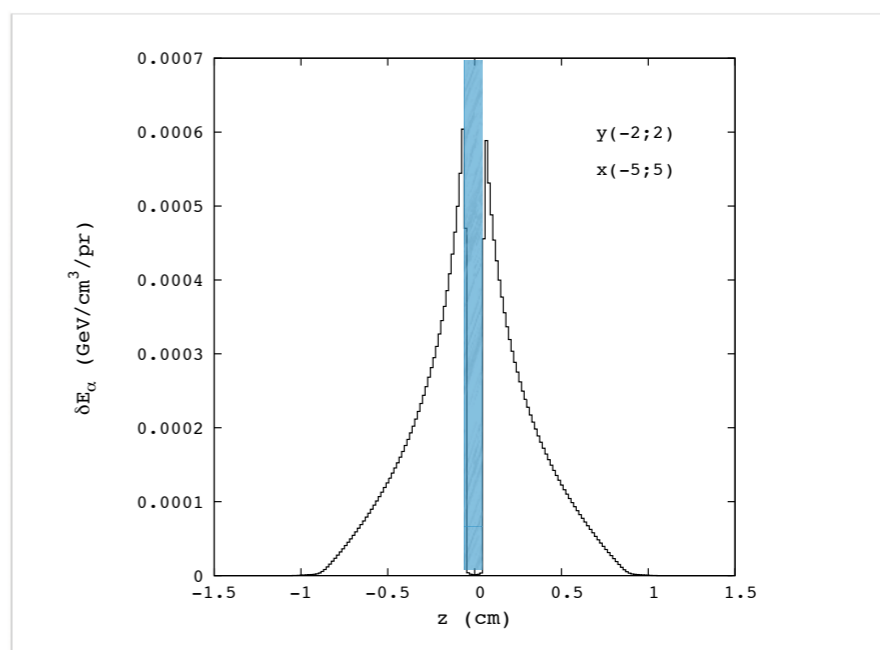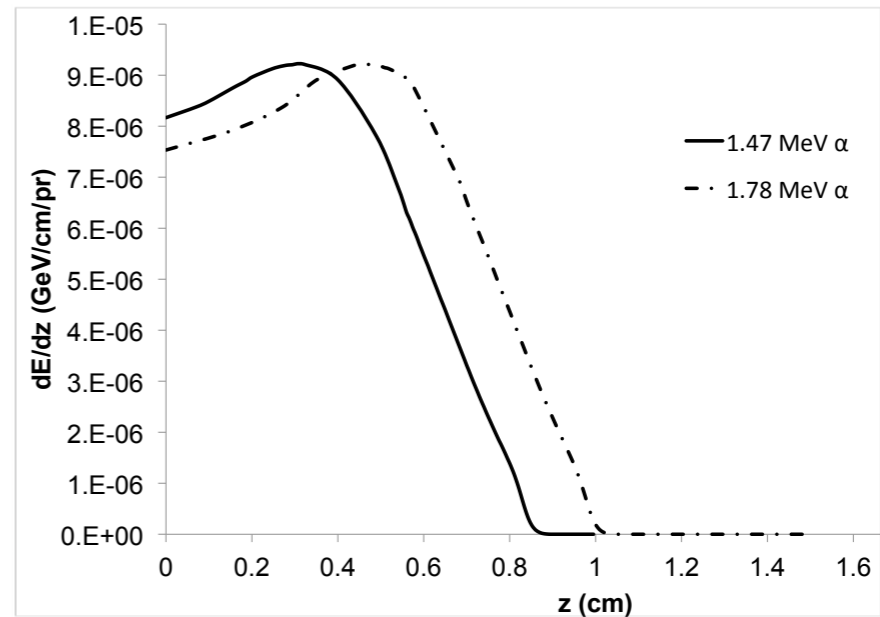
α 3D scatter plots: Particle entering into the gas

These plots refer to the case of a double coated plate with 300nm B-10 film. The angular contribution to efficiency attenuation become an issue for value of the convert thickness above 1000nm, as shown in the following slides
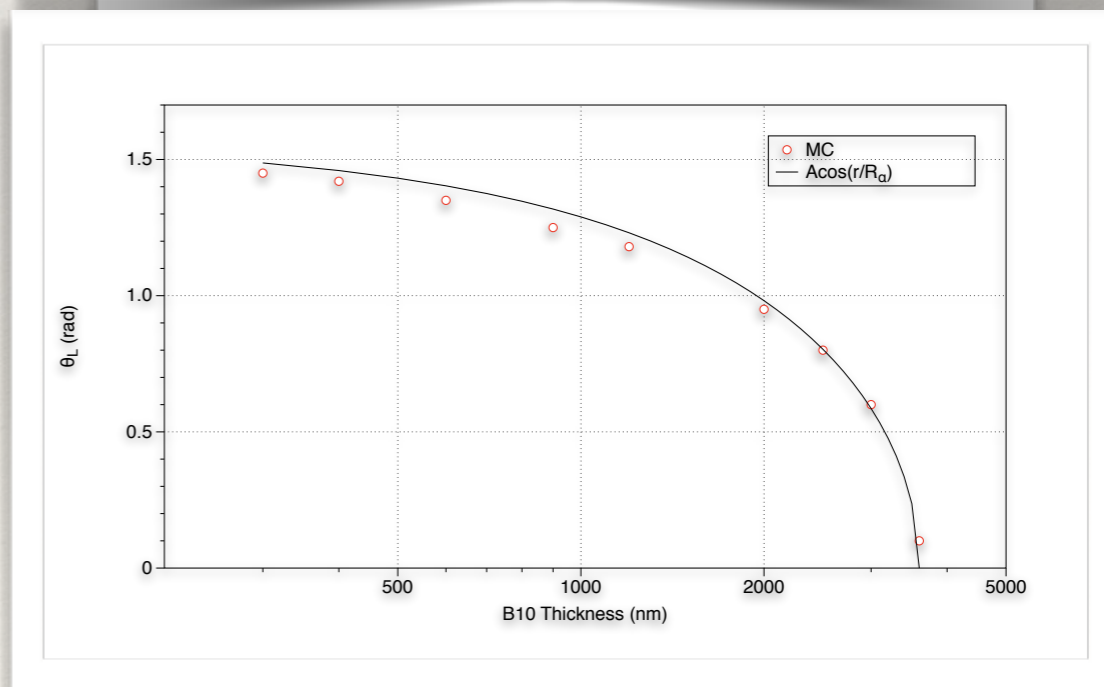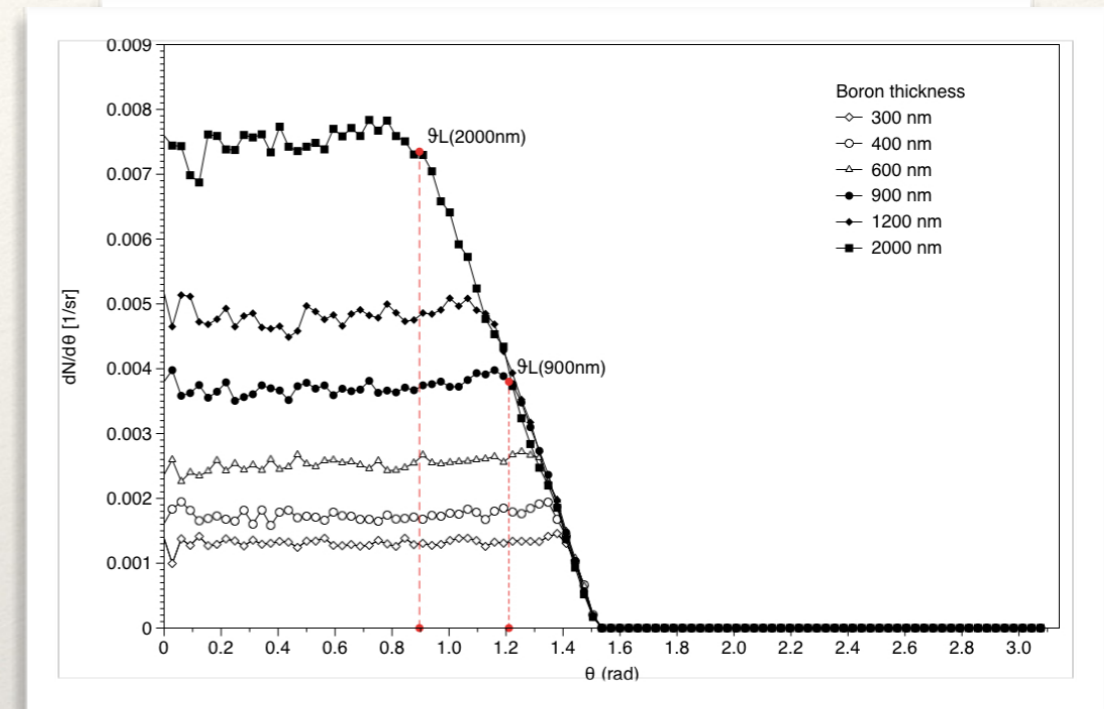

Energy Fluence distribution of alpha entering in MoutGas

dN/dE/pr

alpha into MoutGas

into MoutGas

P

0.115
0.1
0.08
0.06
0.04
0.02
0.00159

angular momenta

Energy Deposition and Angular Distribution in the Gas Around the Single Sheet

❖ Ar/CO_2 mixture (70%/30%) at 1atm: the linear energy deposition features as a broadened Bragg peak whose **maximum for 1.47 MeV α is around 3 mm** (5 mm for 1.78 **α**) and extends up to about 9 mm (11 mm for 1.78 MeV).

❖ In spite of being mono-directional and mono-energetic, the αs and Li7 that emerge from the B-10 layers and enter the gas **have angular isotropic distribution.**

❖ Moreover particles entering into the gas **have a continuous energy spectrum.**

❖ All this is **well taken into account in MC** simulations

❖ The overall energy density profile (energy deposition from αs and Li7 ions, respectively) in the simulated region (solid sheet and gas around) is obtained by cumulating the contributions of all the particles
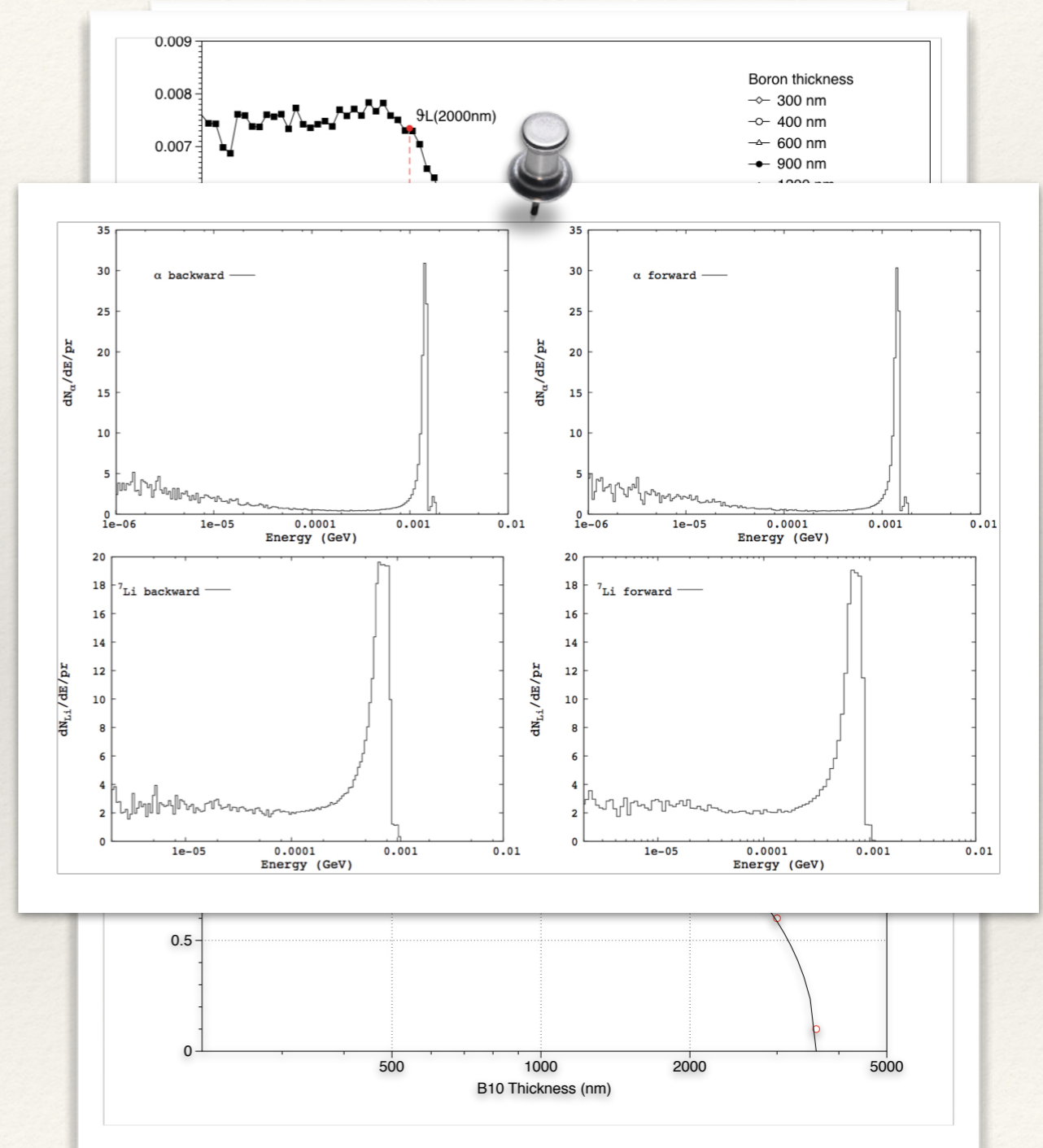
Energy Deposition and Angular Distribution in the Gas Around the Single Sheet

* Ar/CO_2 mixture (70%/30%) at 1atm: the linear energy deposition features as a broadened Bragg peak whose **maximum for 1.47 MeV α is around 3 mm** (5 mm for 1.78 α) and extends up to about 9 mm (11 mm for 1.78 MeV).

* In spite of being mono-directional and mono-energetic, the αs and Li7 that emerge from the B-10 layers and enter the gas **have angular isotropic distribution.**

* Moreover particles entering into the gas **have a continuous energy spectrum.**

* All this is **well taken into account in MC** simulations

* The overall energy density profile (energy deposition from αs and Li7 ions, respectively) in the simulated region (solid sheet and gas around) is obtained by cumulating the contributions of all the particles
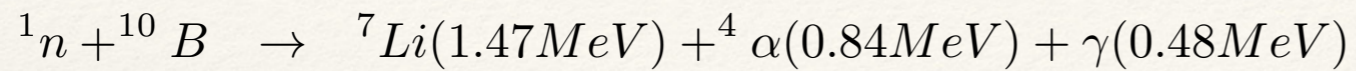
Energy Deposition and Angular Distribution in the Gas Around the Single Sheet

- Ar/CO_2 mixture (70%/30%) at 1atm: the linear energy deposition features as a broadened Bragg peak whose **maximum for 1.47 MeV α is around 3 mm** (5 mm for 1.78 α) and extends up to about 9 mm (11 mm for 1.78 MeV).

- In spite of being mono-directional and mono-energetic, the αs and Li7 that emerge from the B-10 layers and enter the gas **have angular isotropic distribution.**

- Moreover particles entering into the gas **have a continuous energy spectrum.**

- All this is **well taken into account in MC** simulations

- The overall energy density profile (energy deposition from αs and Li7 ions, respectively) in the simulated region (solid sheet and gas around) is obtained by cumulating the contributions of all the particles

Boron Thickness "t" (nm)

$$^1n + ^{10}B \rightarrow \, ^7Li(1.47 MeV) + ^4\alpha(0.84 MeV) + \gamma(0.48 MeV)$$
$$^1n + ^{10}B \rightarrow \, ^7Li(1.78 MeV) + ^4\alpha(1.01 MeV) \; (7\%)$$

$$RR\,[\#reactions/cm3/s] = \Sigma \cdot \Phi \quad \text{where } \Sigma = N\sigma.$$

$$\epsilon = N\sigma \cdot (1 + P_1) \cdot \delta$$

$$P_1 = \frac{I_x}{I_0} = e^{-\Sigma_{tot}x}$$

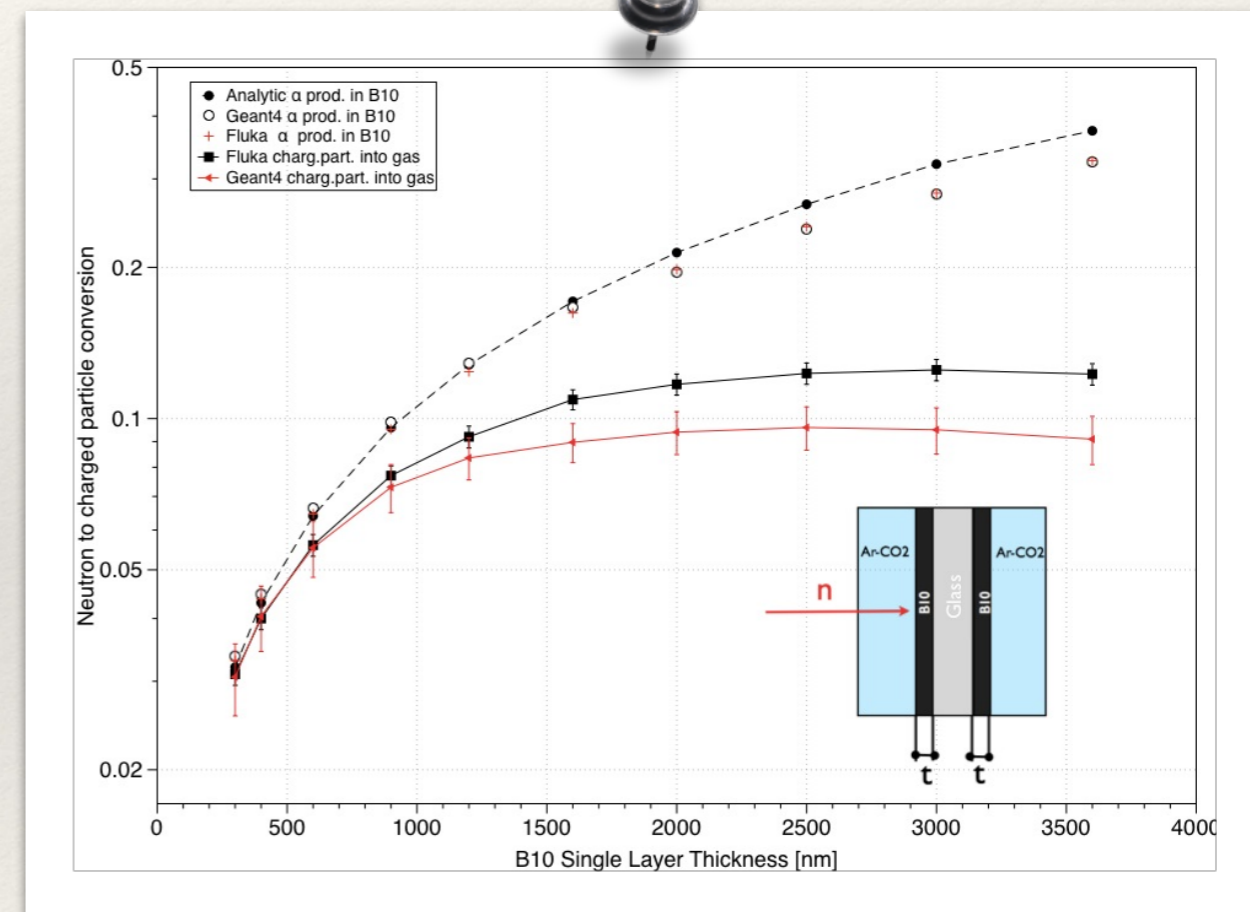**P1 is the fraction of neutrons surviving at depth x (those that do not interact up to x depth).**

Table 1: B10 layer conversion efficiency as a function of thickness

B10-Thicness [nm]	Theoretical %	FLUKA %	Geant4 %	MCNPX %
300	3.2	3.3	3.37	in prog
400	4.3	4.38	4.47	-
600	6.4	6.46	6.63	-
900	9.6	9.52	9.84	-

As the B-10 thickness increases, the **number of charged particles produced differs from the number of charged particles that reach the gas region.** This effect becomes appreciable for B-10 thickness much thiner than the α and Li7 range values. the range of 1.47 MeV αs and 0.84 MeV 7Li ions in 10B is respectively about 3.6 μm and 2 μm
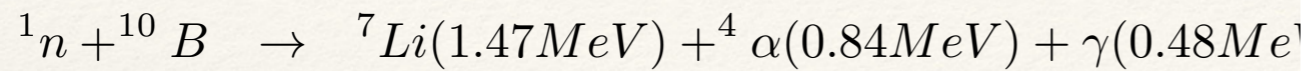
This is explained considering that the **reaction products are emitted quite isotropically**, so that the charged particles that are traveling in a solid angle larger than a certain angle have a **higher probability to be absorbed inside the solid** converter.

Estimated values of αs produced per incident neutron inside the converter layers compared to charged particles (αs and Li7 ions) leaving the B-10 layers and entering into the gas region (FLUKA, GEANT, analytical).

it is apparent that the reaction products will lose energy as they move through the reactive film, thus limiting the energy transferred to the gas region. The finite specific energy loss in the reactive film limits the usable thickness that can be deposited

$$^{1}n + ^{10}B \rightarrow \ ^{7}Li(1.47 MeV) + ^{4}\alpha(0.84 MeV) + \gamma(0.48 MeV)$$

$$^{1}n + ^{10}B \rightarrow \ ^{7}Li(1.78 MeV) + ^{4}\alpha(1.01 MeV) \ (7\%)$$

$$RR\ [\#reactions/cm3/s] = \Sigma \cdot \Phi \quad \text{where } \Sigma = N\sigma.$$

$$\epsilon = N\sigma \cdot (1 + P_1) \cdot \delta$$

$$P_1 = \frac{I_x}{I_0} = e^{-\Sigma_{tot} x}$$

P1 is the fraction of neutrons surviving at depth x (those that do not interact up to x depth).

Table 1: B10 layer conversion efficiency as a function of thickness

B10-Thicness [nm]	Theoretical %	FLUKA %	Geant4 %	MCNPX %
300	3.2	3.3	3.37	in prog
400	4.3	4.38	4.47	-
600	6.4	6.46	6.63	-
900	9.6	9.52	9.84	-

As the B-10 thickness increases, the **number of charged particles produced differs from the number of charged particles that reach the gas region.** This effect becomes appreciable for B-10 thickness much thiner than the **α** and Li7 range values. the range of 1.47 MeV **α**s and 0.84 MeV 7Li ions in 10B is respectively about 3.6 μm and 2 μm

This is explained considering that the **reaction products are emitted quite isotropically**, so that the charged particles that are traveling in a solid angle larger than a certain angle have a **higher probability to be absorbed inside the solid** converter.

Energy Spectrum of alphas from B-10 layer2 toward Moutgas

t=1000 nm
t=300 nm

The continuous tail at lower energy and the broadened peaks in the spectra are due to the energy straggling that particles experience in passing through different thickness of boron before reaching the gas region: indeed, particles emitted at large angles travel over longer tracks inside the B-10 layer, thus loosing much more energy.

Indirectly Derived Electron Density

(collimated spot of thermal neutron beam impinging at the center of the plate)

- ❖ Electron Spatial distribution (elec/cm2/pr) has been derived from the energy deposition density (GeV/cm3/pr) of charged particles dividing by w=28 eV and integrating on the y coordinate.

- ❖ An energy threshold condition has been set in such a way that the energy deposition has been taken into account only for αs with kinetic energy greater than 104 eV (Ionization potential).

- ❖ Finally the spatial binning used for the estimation of the energy deposition spatial bin δy=0.02 for y[-0.1;0.1]

Alpha ionization electron density (elec/cm2/pr) from -0.5cm to -0.4cm
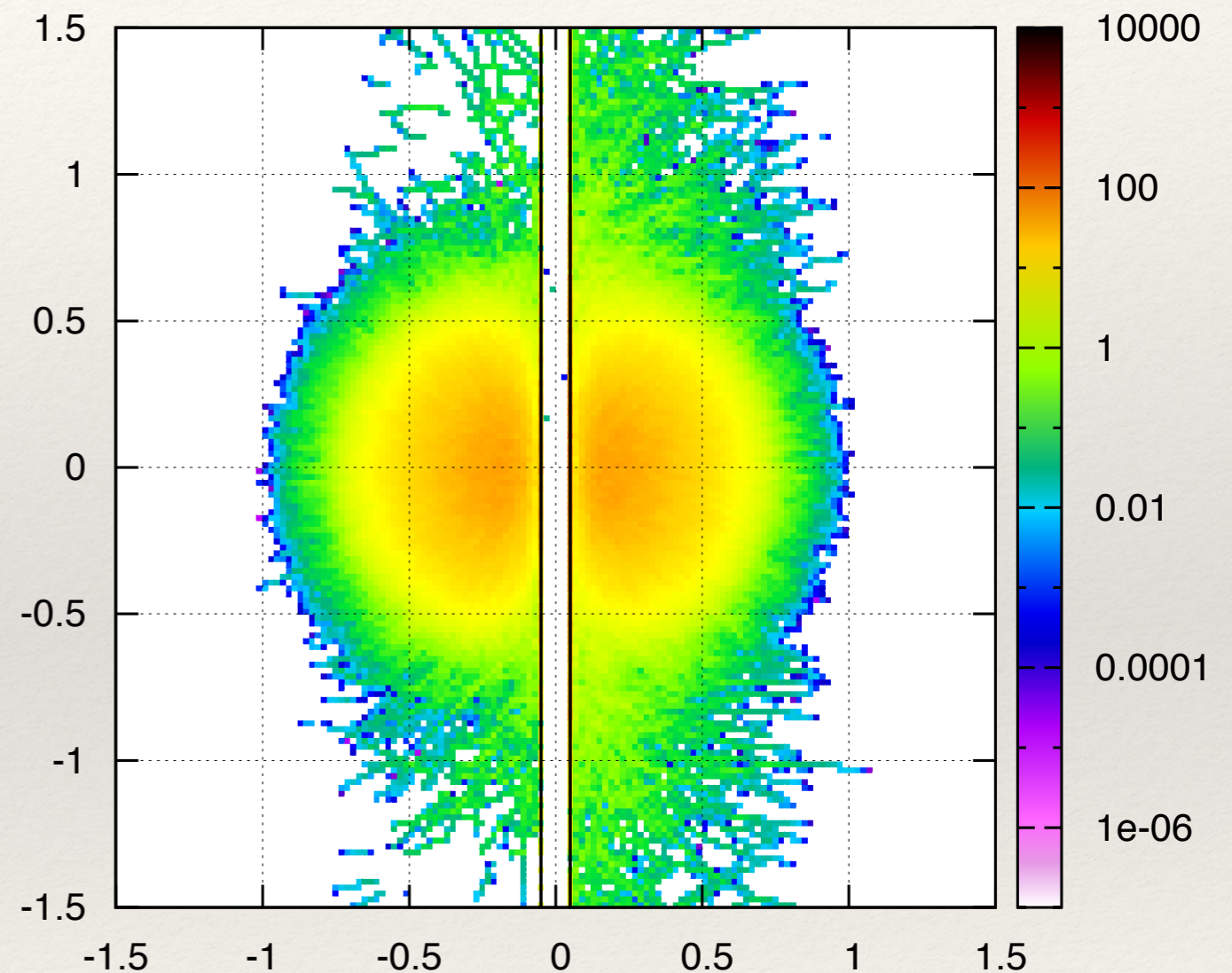
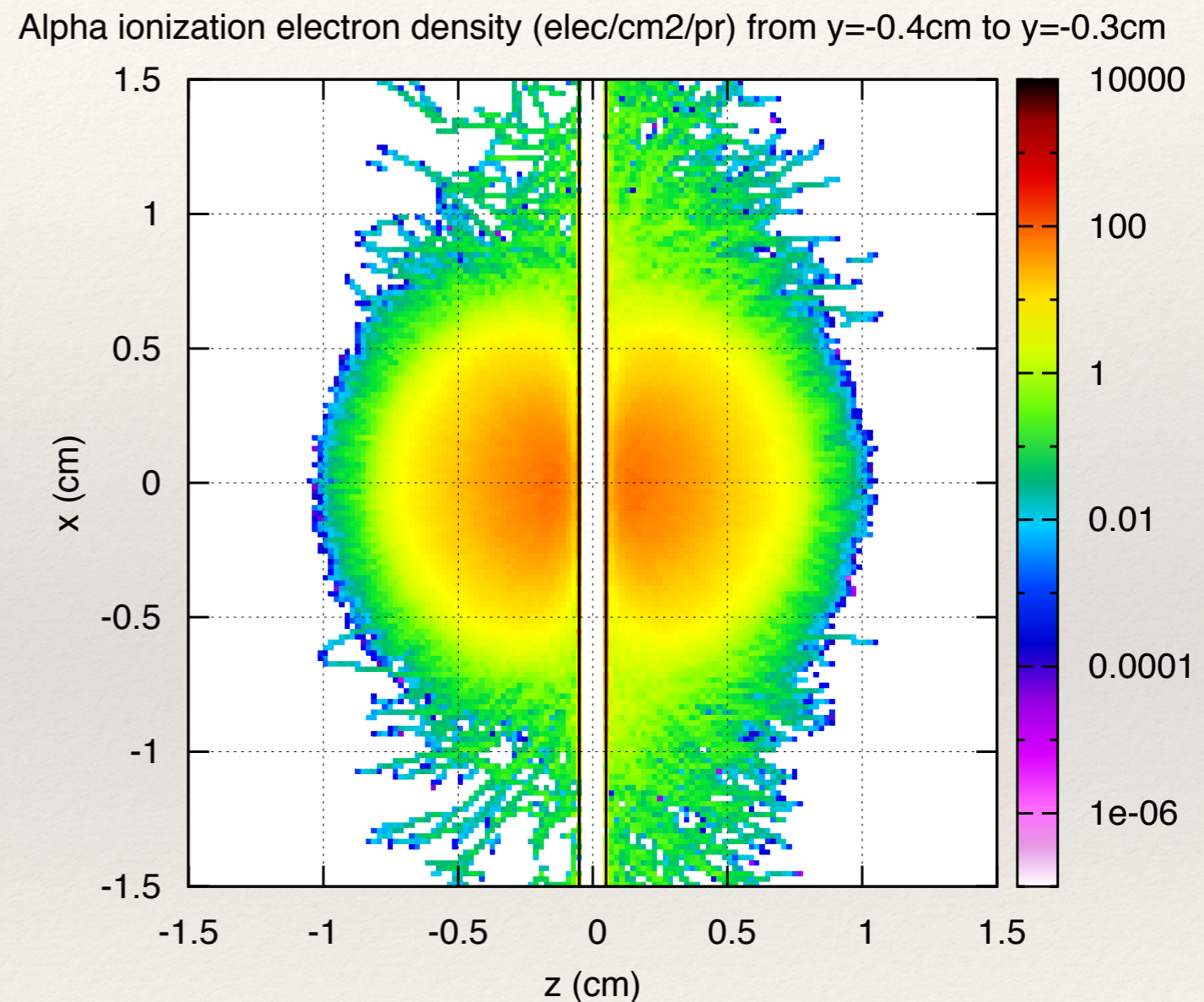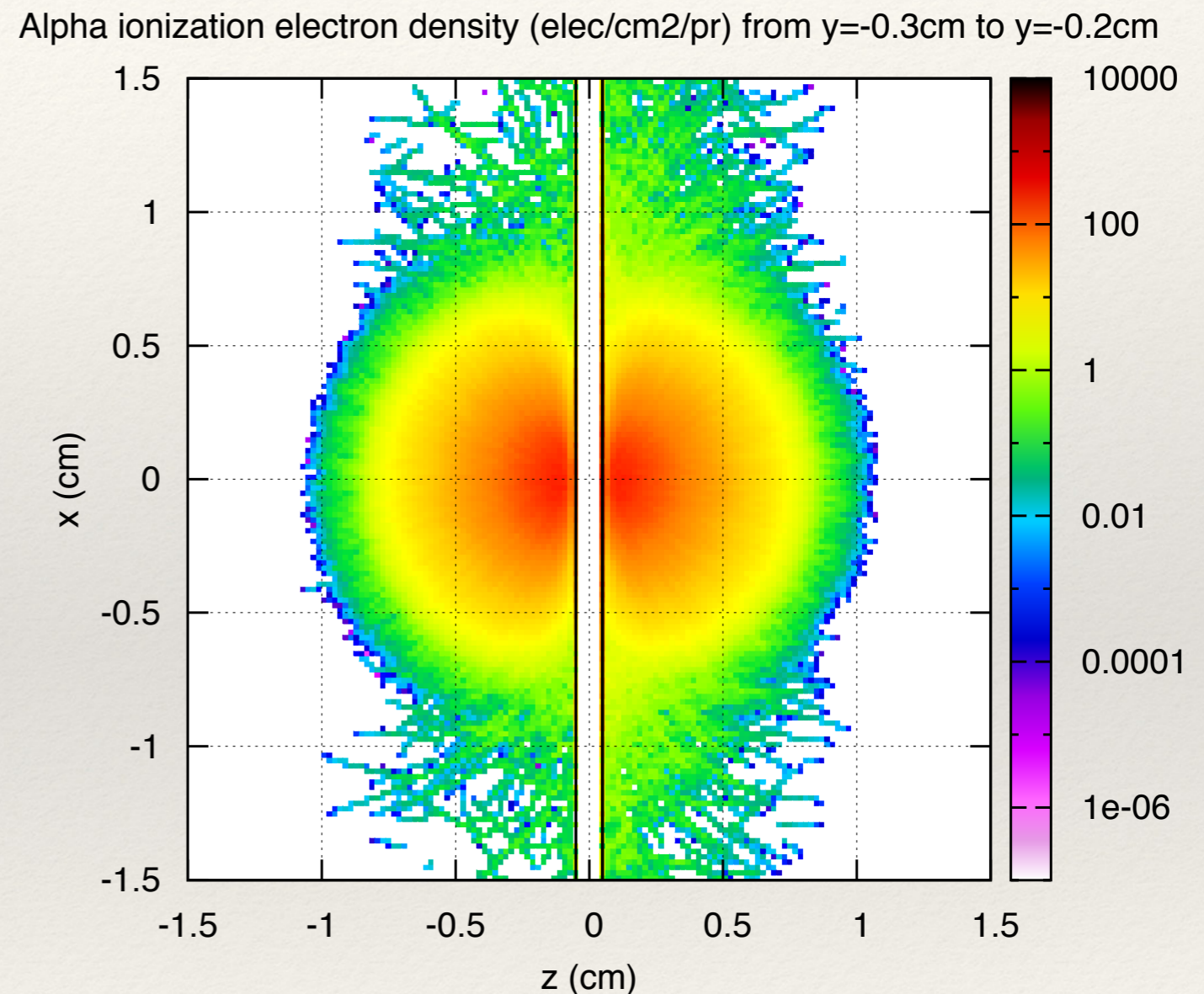**from y=-0.50cm   to y=-0.40cm**

A more accurate and realistic charge distribution in the gas must be obtained taking into account the electric field that is going to be introduced in the ongoing refined simulations

Indirectly Derived Electron Density

(collimated spot of thermal neutron beam impinging at the center of the plate)

- ❖ Electron Spatial distribution (elec/cm2/pr) has been derived from the energy deposition density (GeV/cm3/pr) of charged particles dividing by w=28 eV and integrating on the y coordinate.

- ❖ An energy threshold condition has been set in such a way that the energy deposition has been taken into account only for αs with kinetic energy greater than 104 eV (Ionization potential).

- ❖ Finally the spatial binning used for the estimation of the energy deposition spatial bin δy=0.02 for y[-0.1;0.1]

Alpha ionization electron density (elec/cm2/pr) from y=-0.4cm to y=-0.3cm
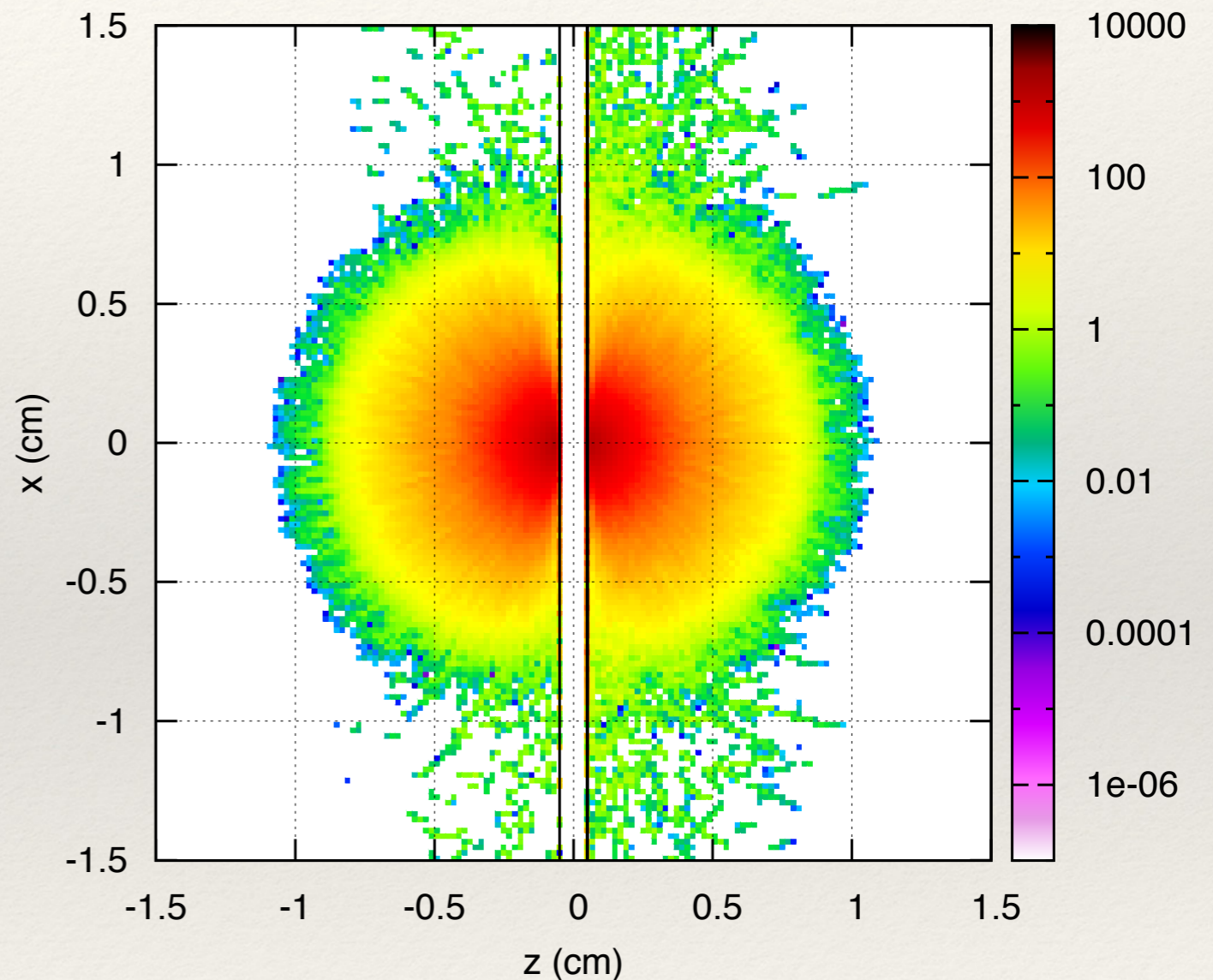
from y=-0.40cm   to y=-0.30cm

A more accurate and realistic charge distribution in the gas must be obtained taking into account the electric field that is going to be introduced in the ongoing refined simulations

Indirectly Derived Electron Density

(collimated spot of thermal neutron beam impinging at the center of the plate)

- ❖ Electron Spatial distribution (elec/cm2/pr) has been derived from the energy deposition density (GeV/cm3/pr) of charged particles dividing by w=28 eV and integrating on the y coordinate.

- ❖ An energy threshold condition has been set in such a way that the energy deposition has been taken into account only for αs with kinetic energy greater than 104 eV (Ionization potential).

- ❖ Finally the spatial binning used for the estimation of the energy deposition spatial bin δy=0.02 for y[-0.1;0.1]

Alpha ionization electron density (elec/cm2/pr) from y=-0.3cm to y=-0.2cm
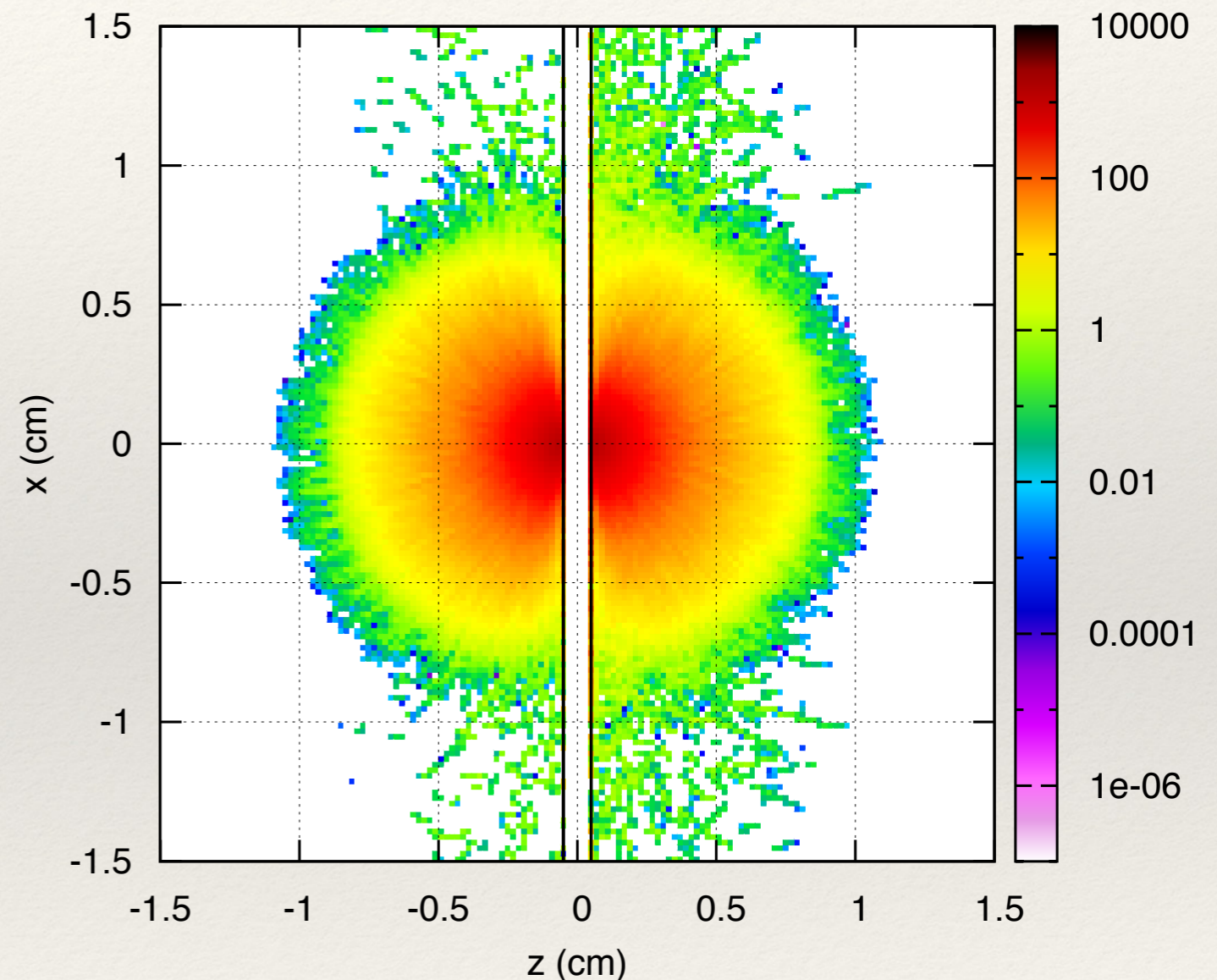
from y=-0.30cm   to y=-0.20cm

A more accurate and realistic charge distribution in the gas must be obtained taking into account the electric field that is going to be introduced in the ongoing refined simulations

Indirectly Derived Electron Density

(collimated spot of thermal neutron beam impinging at the center of the plate)

❖ Electron Spatial distribution (elec/cm2/pr) has been derived from the energy deposition density (GeV/cm3/pr) of charged particles dividing by w=28 eV and integrating on the y coordinate.

❖ An energy threshold condition has been set in such a way that the energy deposition has been taken into account only for αs with kinetic energy greater than 104 eV (Ionization potential).

❖ Finally the spatial binning used for the estimation of the energy deposition spatial bin δy=0.02 for y[-0.1;0.1]

Alpha ionization electron density (elec/cm2/pr) from y=-0.1cm to y=-0.08cm
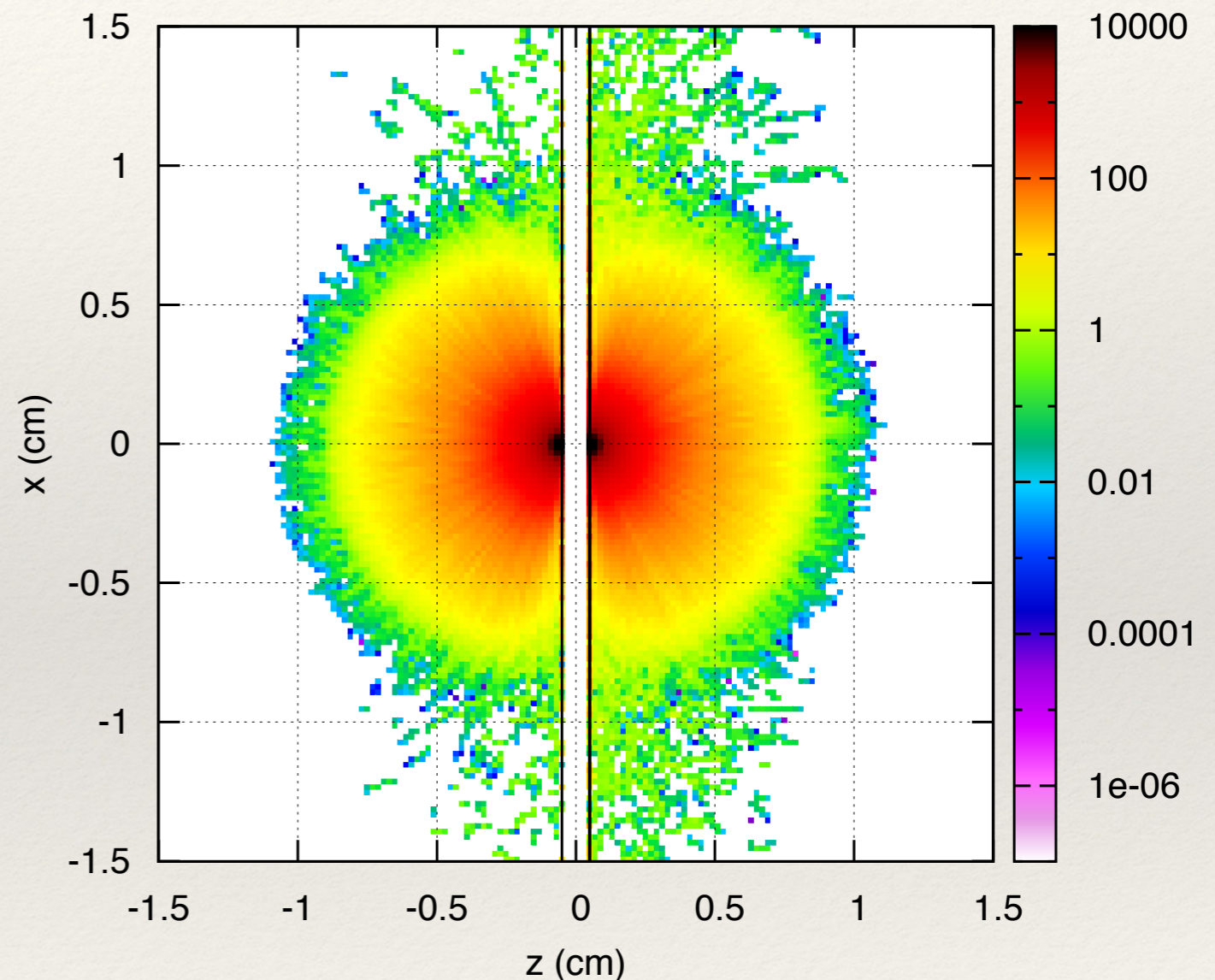
from y=-0.10cm   to y=-0.08cm

A more accurate and realistic charge distribution in the gas must be obtained taking into account the electric field that is going to be introduced in the ongoing refined simulations

Indirectly Derived Electron Density

(collimated spot of thermal neutron beam impinging at the center of the plate)

- ❖ Electron Spatial distribution (elec/cm2/pr) has been derived from the energy deposition density (GeV/cm3/pr) of charged particles dividing by w=28 eV and integrating on the y coordinate.

- ❖ An energy threshold condition has been set in such a way that the energy deposition has been taken into account only for αs with kinetic energy greater than 104 eV (Ionization potential).

- ❖ Finally the spatial binning used for the estimation of the energy deposition spatial bin δy=0.02 for y[-0.1;0.1]

Alpha ionization electron density (elec/cm2/pr) from y=-0.1cm to y=-0.08cm

from y=-0.06cm   to y=-0.04cm

A more accurate and realistic charge distribution in the gas must be obtained taking into account the electric field that is going to be introduced in the ongoing refined simulations

Indirectly Derived Electron Density

(collimated spot of thermal neutron beam impinging at the center of the plate)

- ❖ Electron Spatial distribution (elec/cm2/pr) has been derived from the energy deposition density (GeV/cm3/pr) of charged particles dividing by w=28 eV and integrating on the y coordinate.

- ❖ An energy threshold condition has been set in such a way that the energy deposition has been taken into account only for αs with kinetic energy greater than 104 eV (Ionization potential).

- ❖ Finally the spatial binning used for the estimation of the energy deposition spatial bin δy=0.02 for y[-0.1;0.1]

Alpha ionization electron density (elec/cm2/pr) from y=0.00cm to y=0.02cm

from y=-0.02cm   to y=0.00cm

A more accurate and realistic charge distribution in the gas must be obtained taking into account the electric field that is going to be introduced in the ongoing refined simulations

Multiple Sheet Detector Geometric Configuration Optimization

Optimal configuration with respect to maximize the number of charged particles that can ionise the gas region

### A. Optimal distance among stacked plates (coating thickness and the volume fixed)

Energy deposited by the charged particles **in the gas** as a function of the **number of sheets** in a fixed volume with two-side 300nm B-10 thickness. Four cases have been simulated: 5, 10, 15, 18 (gas gap, respectively, 1cm , 0.5 cm, 0.3125cm and 0.25cm)
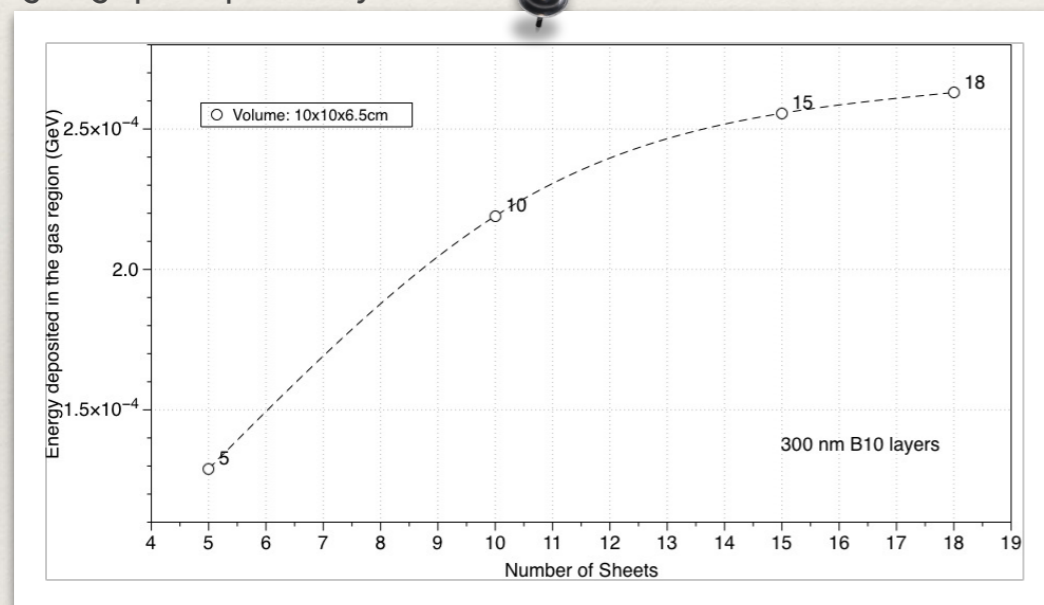
The total energy deposition in the considered fixed volume is expected to **increase of about 70% doubling the number of plates from 5 to 10** (i.e. reducing the gap from 1 to 0.5 cm), but less than 20% going from 10 to 18 (i.e. reducing the gap from 0.5 cm to 0.25 cm).

A detailed estimation of the energy deposited in each gas region in between two adjacent sheets indicates that more than 95% of the total kinetic energy of all αs and 7Li ions is deposited within 0.5 cm from the sheet 10B external surface. **An optimum gap of 6 mm has been assessed**
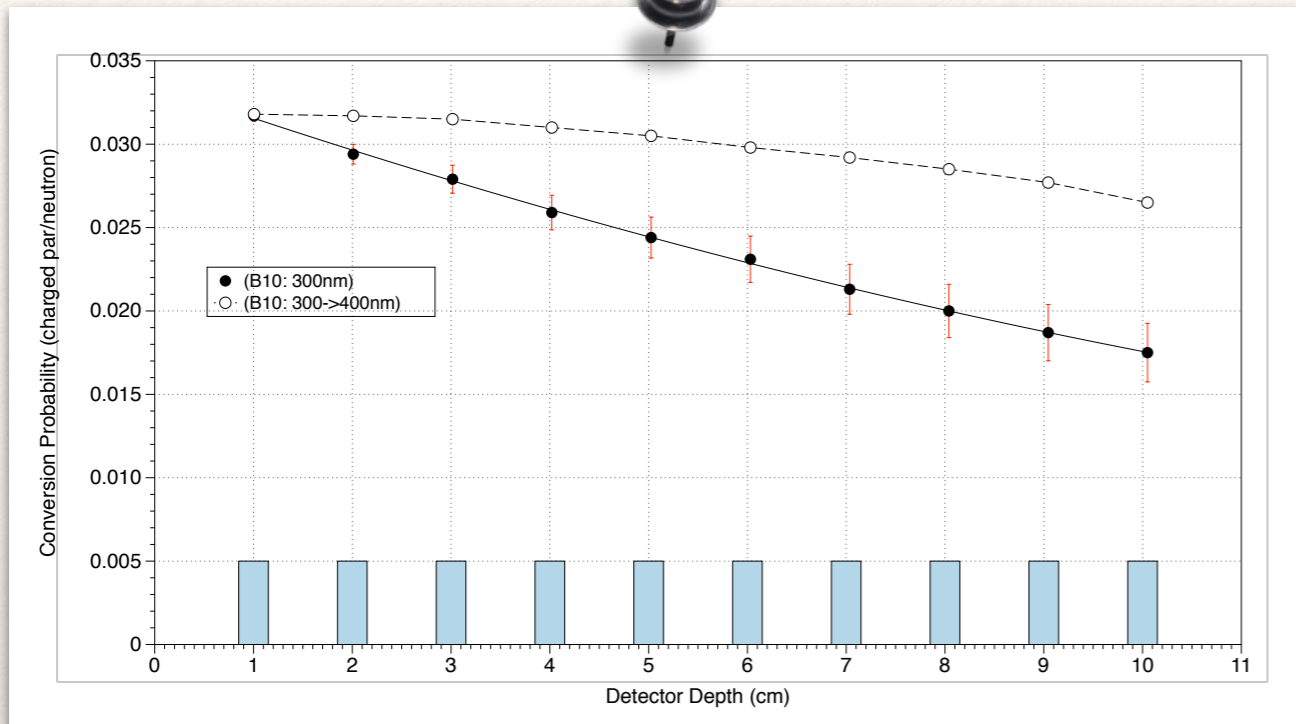
### B. Optimal thickness of the coating (fixing the number of sheets and the relative distance)
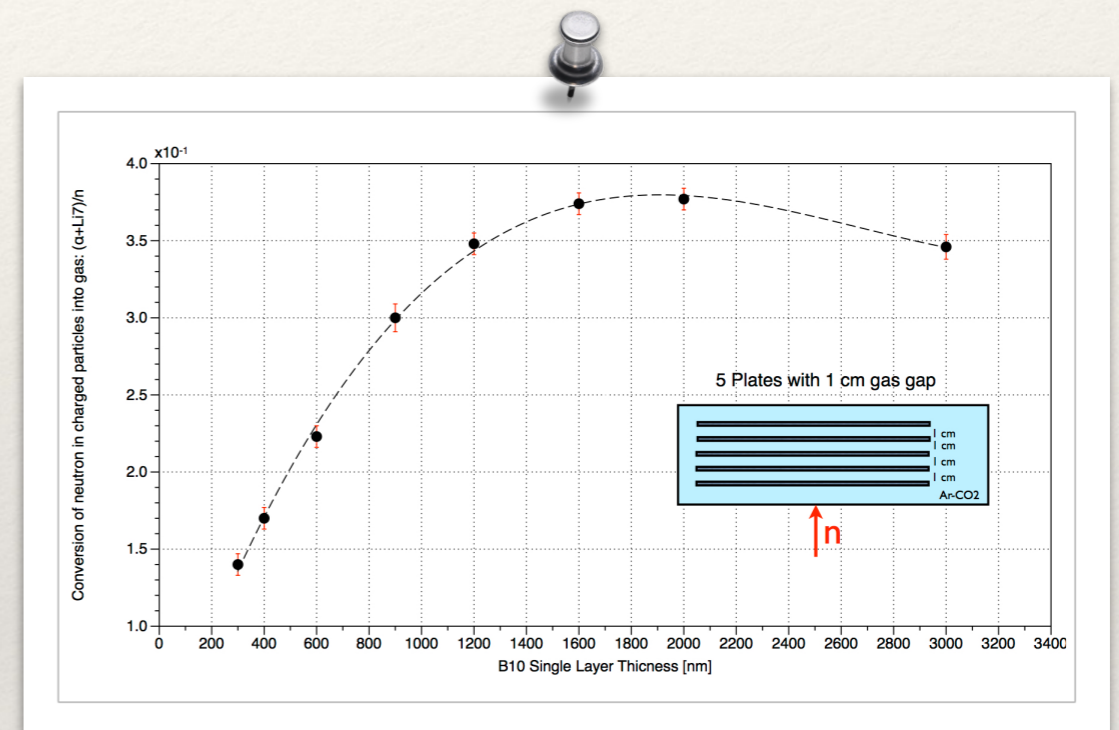
This analysis shows that an **optimum B-10 thickness** exists for a given volume and number of sheets: **in case of 5 sheets it is around 1800 nm**.

"Shadowing Effect": Envisaging a Solution

*Measurements and Simulations for thermal neutrons*

workshop ILL – 2012-03-13/14

Efficiency per cell

3 μm B$_4$C on Si
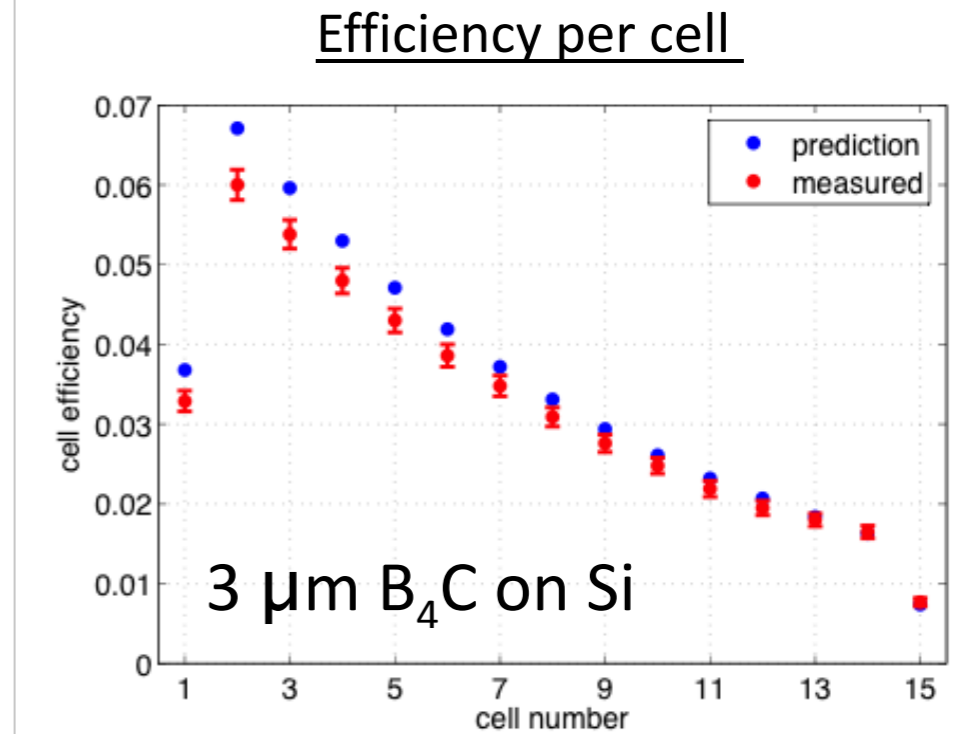
2012-03-13/14 | carina.hoglund@esss.se

* ❖ Estimated conversion efficiency in the case of 10 sheets detector (1cm apart 300nm B-10 thickness 2-side coated).
* ❖ Monochromatic thermal neutron (25 meV)
* ❖ The shadowing effect can be mitigated by using a non-constant B-10 coating along the neutron path inside the detector.

Each grid: 17 Al-blades, 20 x 80 x 0.5 mm³

Single side coated (not mounted)

15 x 2-side coated

Single side coated (not mounted)
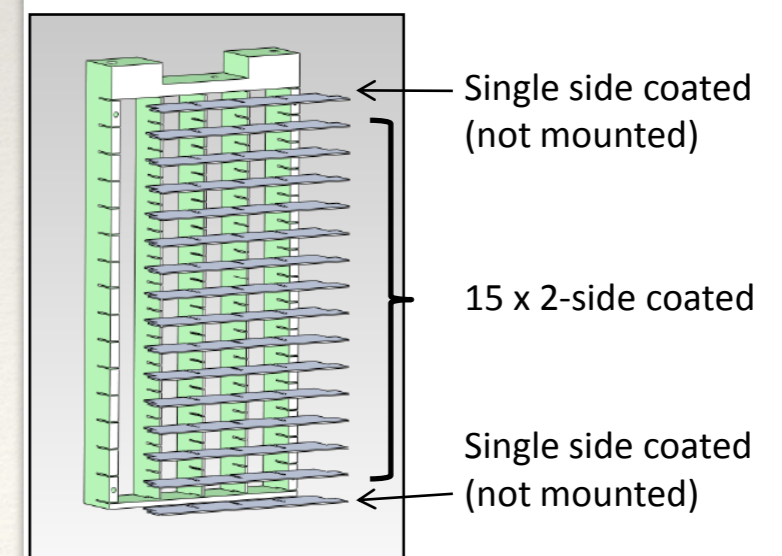
MC predictions and experimental results: Comparison for 5 sheets 300 nm B-10 detector at ENEA TRIGA

- TRIGA reactor at the ENEA-Centro Ricerche Casaccia (Rome):

- The reactor can be operated at different powers from a few Watt to 1 MW with a neutron flux of about 2 E+6 n/cm2/s at the maximum power, whose spectrum is shown in the picture
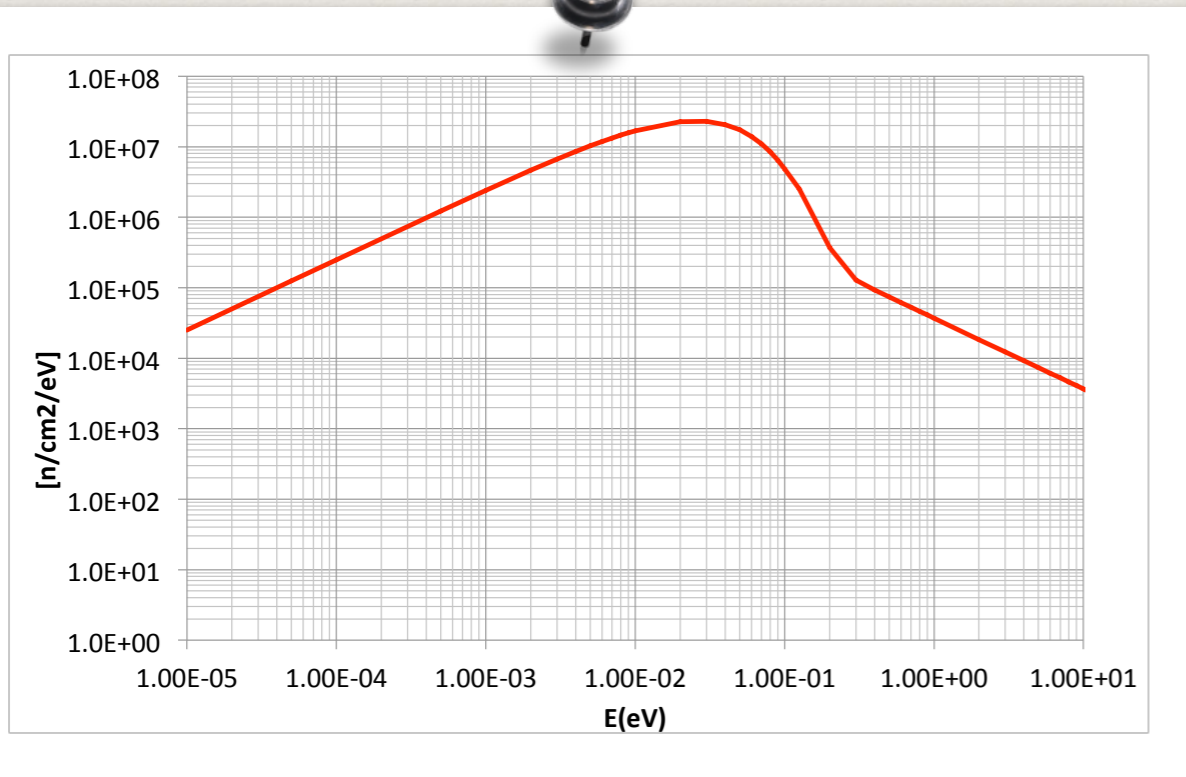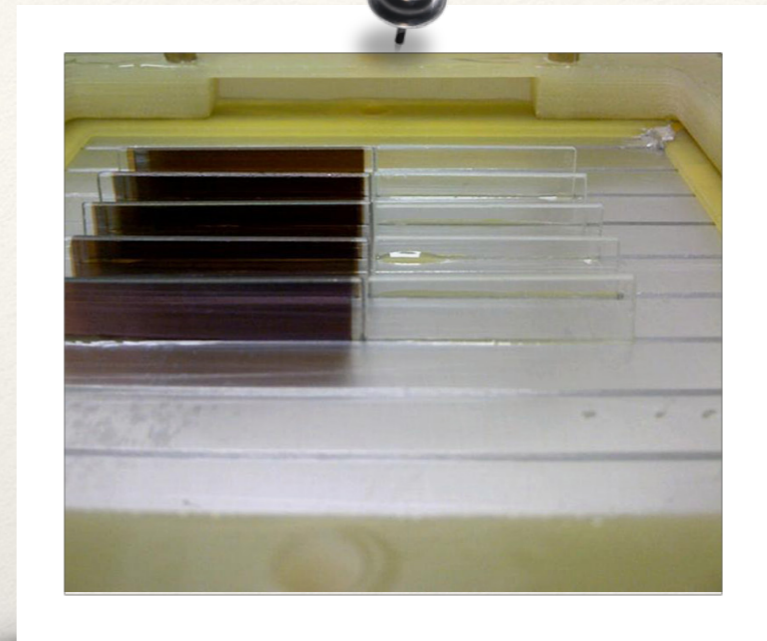

Conv. Efficiency	MC	Exp
$\varepsilon[\%]$	7.4±0.6	4.6±0.5

Difference between MC prediction and the measurement likely due to:

- the overall **charge production/amplification/threshold in the detector stages**, that is not included in the MC model;

- a **possible contamination of B_2O_3** and the reduced density of the films with respect to the bulk value in the conversion film (importance of the spectrometric analysis of the layer)

- The **experimental contribution of the external face of the first sheet** is lost, whilst it has been taken into account in the simulation

LiF: Single Plate Preliminary Results

- ❖ Conversion efficiency vs thickness (as starting point, same thickness as B-10 detector)

- ❖ Energy spectra of escaping charged particles versus thickness

- ❖ Efficiency vs impinging neutron energy for a defined thickness
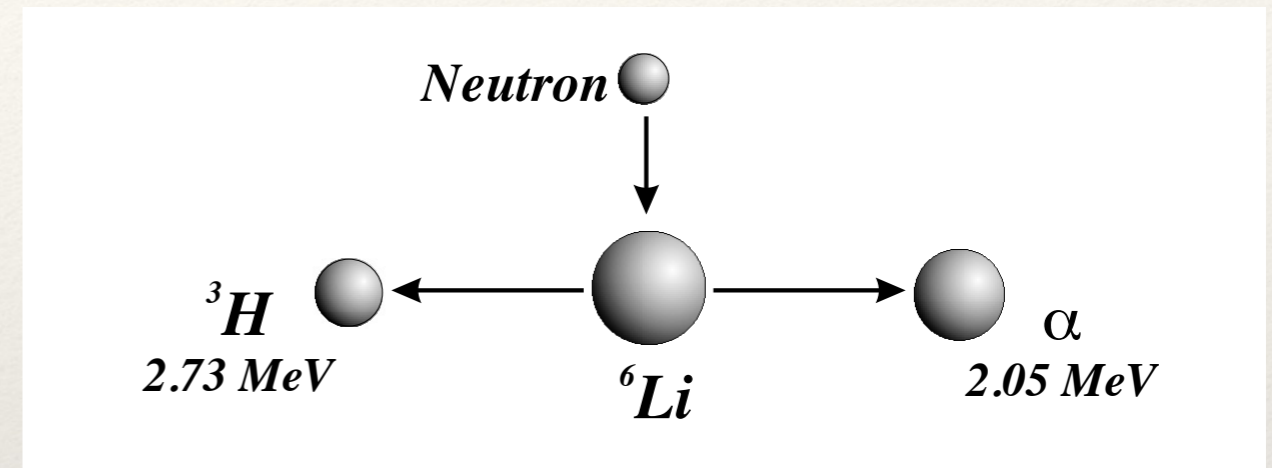
The Li6(n,α)H3 reaction emits **2.73 MeV triton** (3H) and a **2.05 MeV α** particle upon the absorption of a thermal neutron.

One popular form of Li6 is the **stable compound LiF** with molecular density 6.12 E +22 molecules/cm3, hence the atomic density of Li6 amounts to the same. **The mass density of LiF is 2.54 g/cm3. The microscopic thermal cross section of Li6 is 940 b**

Lithium Fluoride also has a very high electrical resistance

LiF Single Plate Efficiency

❖ LIF: 50% in atoms enriched Li and 50% Fluorine. Enriched Li: 94% Li-6 and 4% Li7

❖ The plot values have been obtained for a thermal neutron beam

Excellent agreement between Geant4 and Fluka conversion efficiency prediction
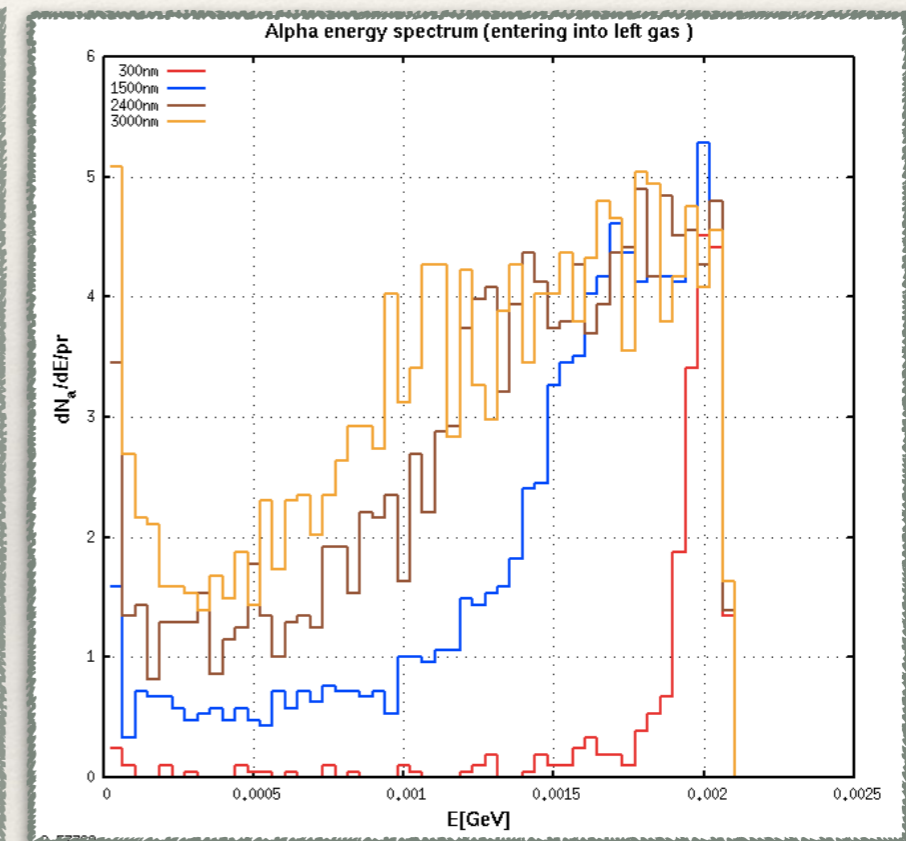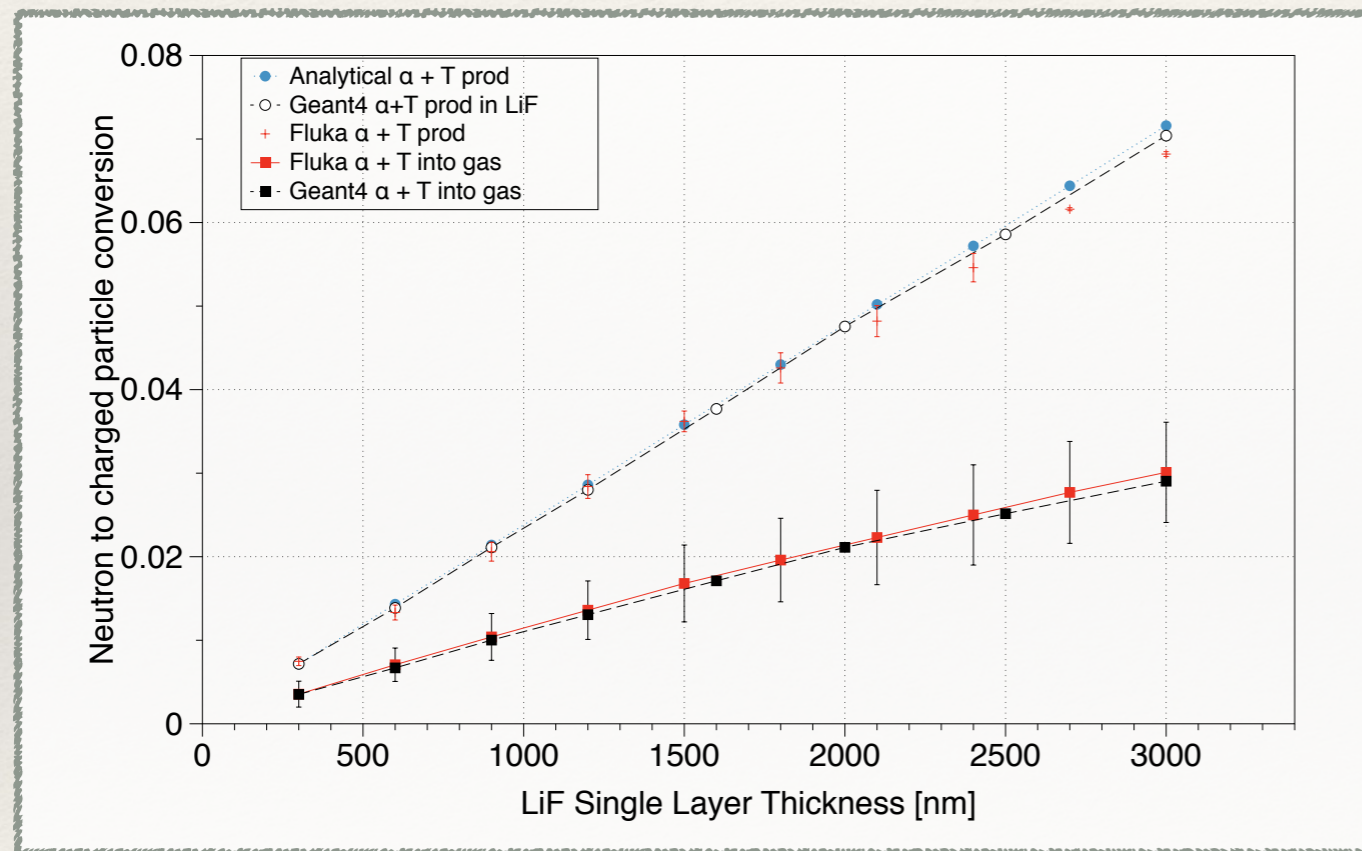
❖ The conversion efficiency is intended the ratio between the total charted particles (triton, α) that enter into gas region surrounding the plate per unit neutron impinging on the converte layer.

❖ The actual detector efficiency, at the end, depends strongly on the charged particles kinetic energy with which they enter the gas region all around and their ability to ionise.

B-10 and Li-6 conversion efficiency comparison
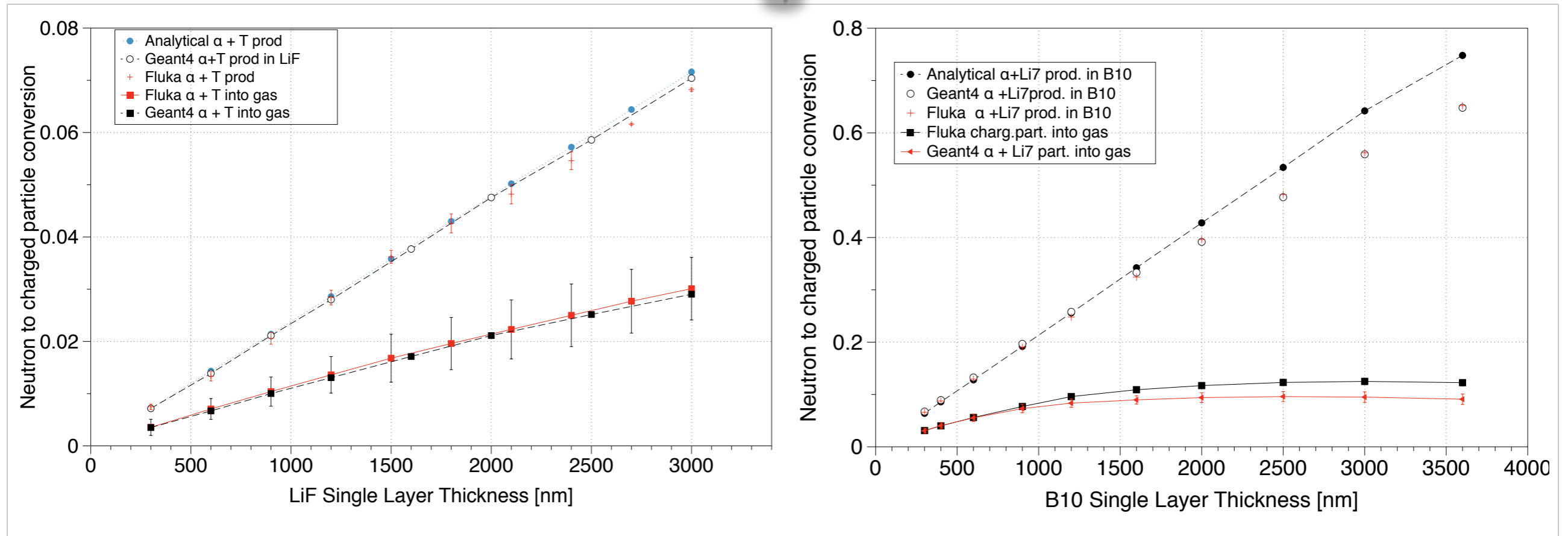
- ❖ At low thickness the difference is essentially related to the absorption cross section ratio, taking into account the actual percentage of Li-6 is (0.5 *0.96)
- ❖ $\sigma\_B\text{-}10/(\sigma\_L6*0.48)= 3800/(940*0.48)=$ **0.84**
- ❖ Ratio (α+Li7 in gas/ α+Triton in gas)= 3.06e-2/3.519e-3=**0.86**
- ❖ This is no longer true at higher energies where the particle absorption play a relevant role
- ❖ Main difference on the Li7 and Triton behaviour in terms of escaping probability

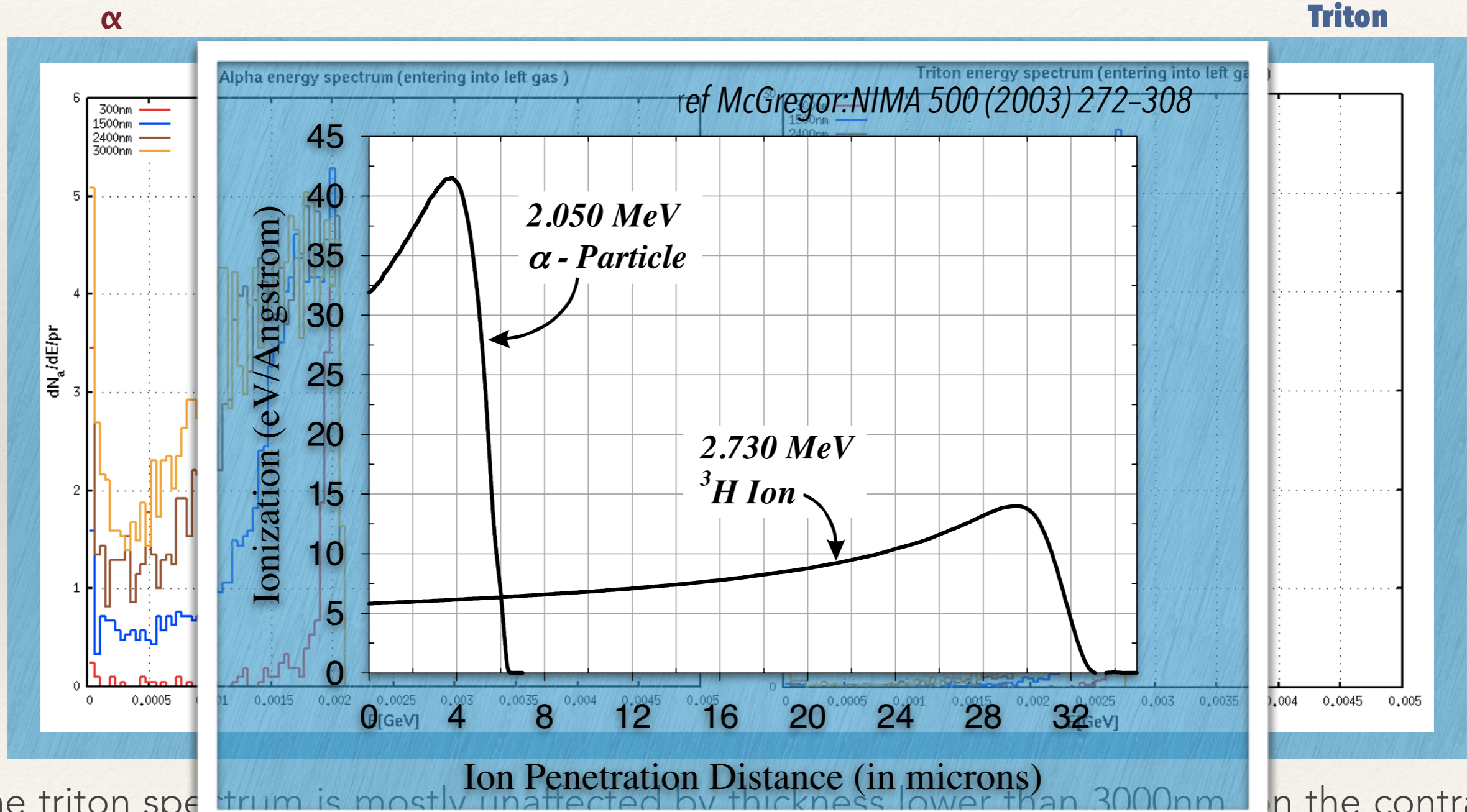# LiF: Secondary Charged Particles Energy Spectrum

Results refer to simulation of a thermal beam on a doubled coated plate with LiF thickness1200nm
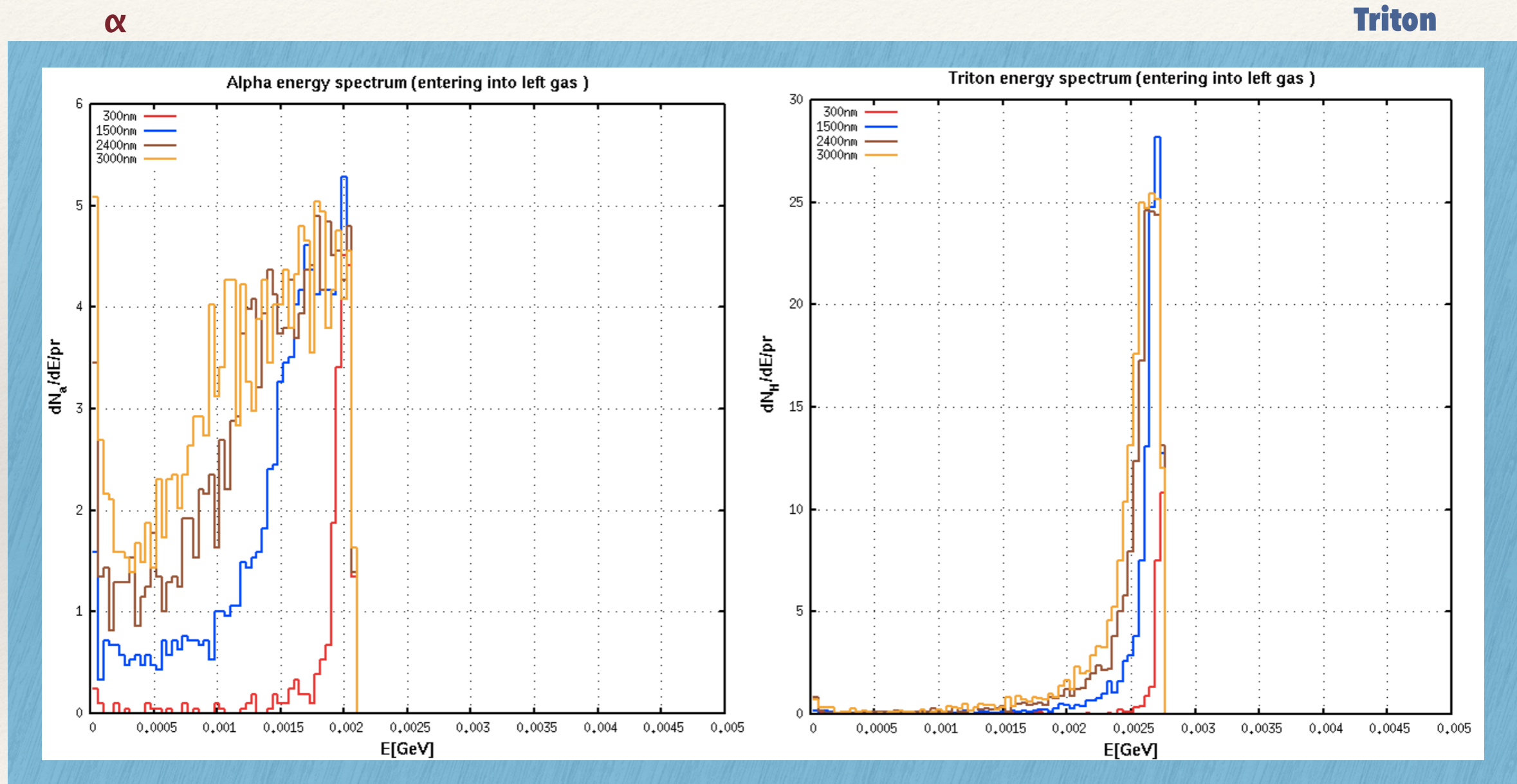
The triton spectrum is mostly unaffected by thickness lower than 3000nm, on the contrary α particles experience an important straggling at low energy starting from 1200 nm

LiF: Secondary Charged Particles Energy Spectrum

Results refer to simulation of a thermal beam on a doubled coated plate with LiF thickness1200nm

α   **Triton**

ref McGregor:NIMA 500 (2003) 272–308

2.050 MeV
α - Particle

2.730 MeV
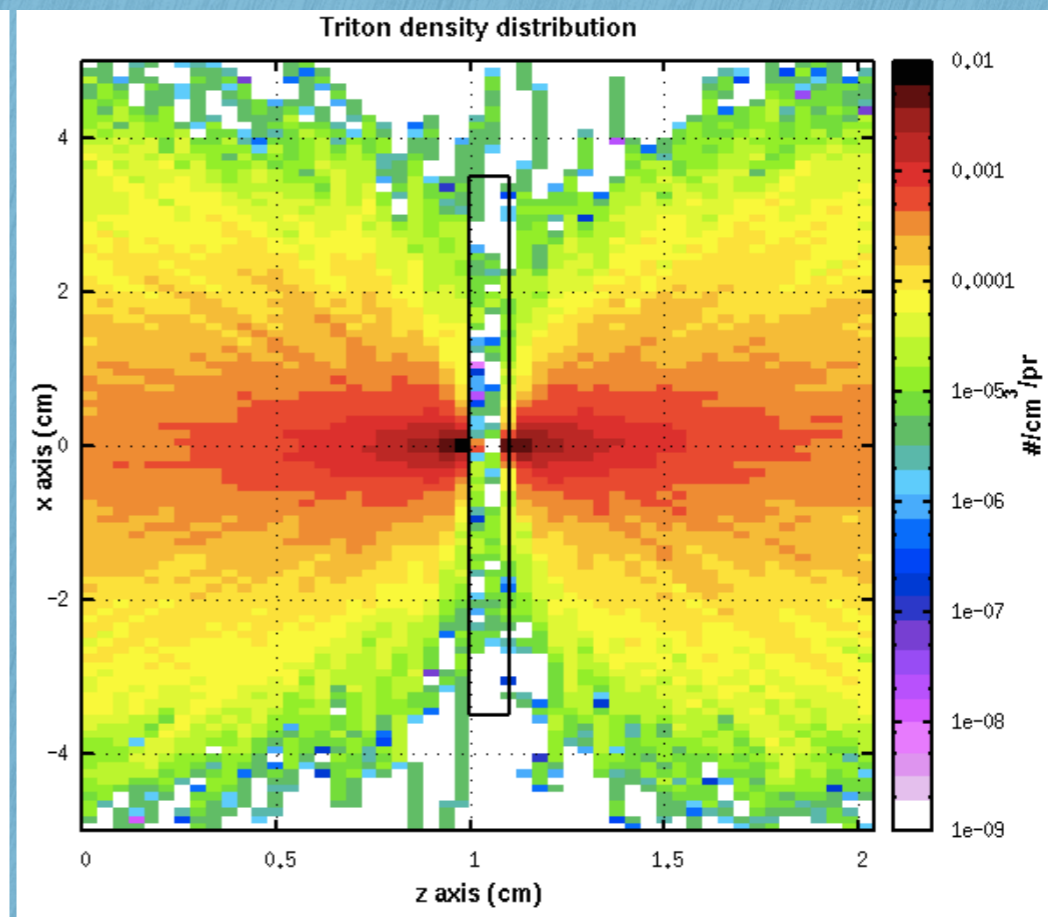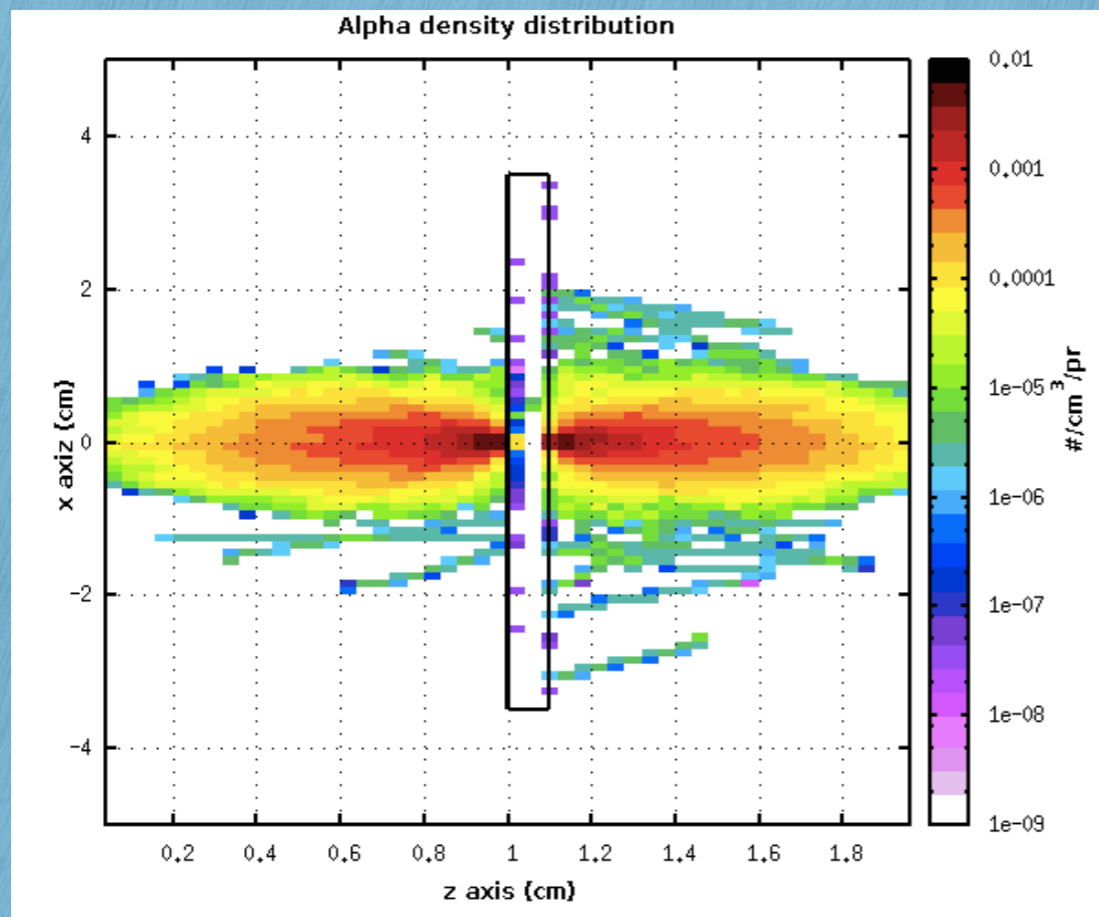*³H Ion*

Ion Penetration Distance (in microns)

The triton spectrum is mostly unaffected by thickness lower than 3000nm on the contrary α particles experience an important straggling at low energy starting from 1200 nm

LiF: Particle Density Distribution

LIF: 50% in atoms enriched Li and 50% Fluorine. Enriched Li: 94% Li-6 and 4% Li7

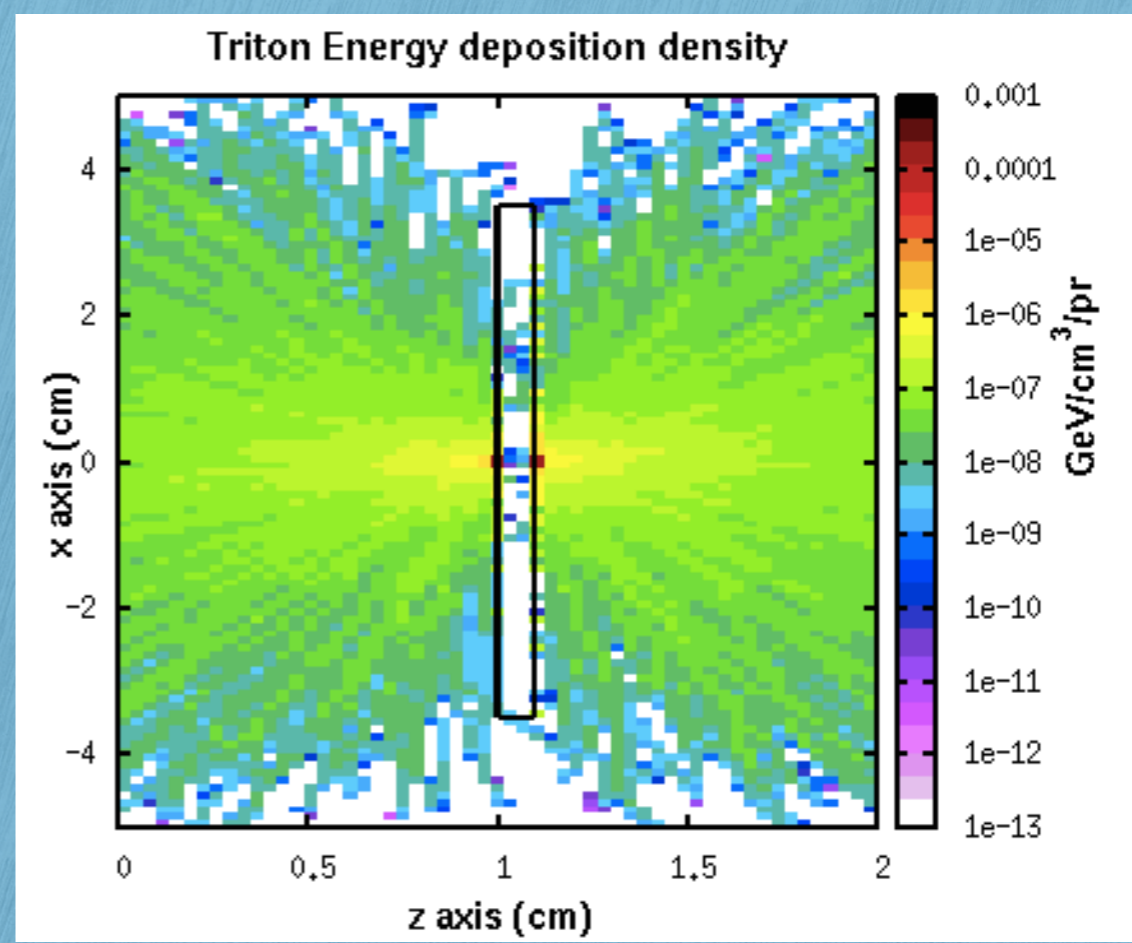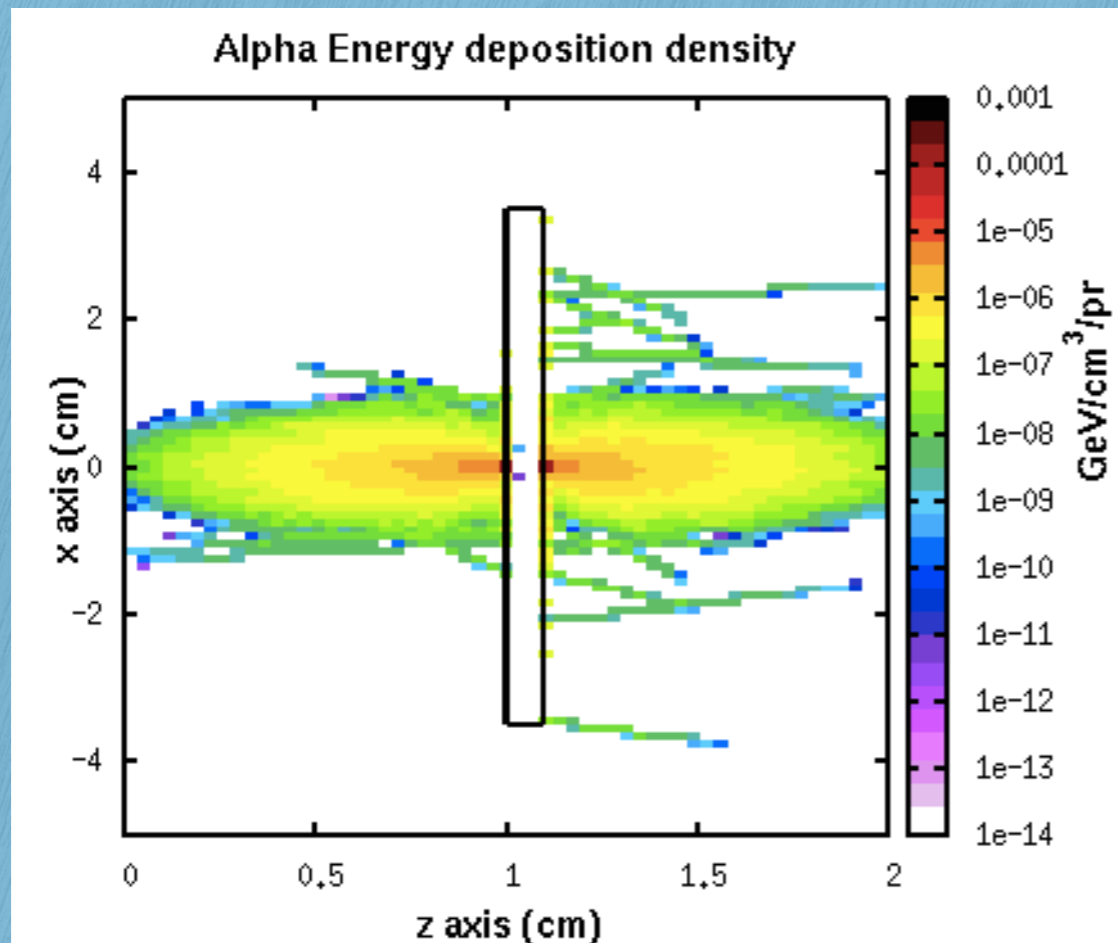# LiF: Particle Energy Deposition in the Simulated Volume

LIF: 50% in atoms enriched Li and 50% Fluorine. Enriched Li: 94% Li-6 and 4% Li7

α   Triton

Tritium particles mostly pass unaffected trough the gas volume considered (5cm x5cm x 5cm). Fluka cannot describe properly the low electron ionisation electron produced in the gas (electron below 1000 eV are not transported), The lowest limit of electron transport in geant is 250 eV. The energy density deposition from triton in gas is more than an order of magnitude less than from α particles

Conclusions

* MC simulations allowed to individuate the optimum converter thickness and gas gap among stacked plates for the "GemSide-On" detector configuration, estimating the charged ions (α, Li7) entering into the gas region

* **FLUKA and Geant4** predictions on conversion efficiency in LiF and B-10 **are in agreement** (with some minor discrepancies in the case of B-10 layer, that have to be further investigated)

* **Other codes** (MCNPX/PHITS) **will be tested** to perform an accurate MC comparison. This will be done in the frame of a project that foresees the major MC codes comparison for special cases with interest in Health physics and neutron metrology applications.

* Conversion efficiency versus neutron energy is in progress, both for B-10 and LiF, as well as angular incidence and other major parameters sensitivity studies are ongoing.

* Optimisation of the interface of MC results with specialised gas detector code for ionization propagation in gas detector (Garfield) is in progress

Thank You for Your Attention!